Distinct mechanisms regulate cell migration in confined versus unconfined spaces

by

Wei-Chien Hung

A dissertation submitted to the John Hopkins University in conformity with the requirements for the degree of Doctor of Philosophy of Chemical and Biomolecular Engineering

Baltimore, Maryland

October 2014

ABSTRACT

Using a microchannel assay, we demonstrate that cells adopt distinct signaling strategies to modulate cell migration in different physical microenvironments. We studied α4β1 integrin-mediated signaling, which regulates cell migration pertinent to embryonic development, leukocyte trafficking and melanoma invasion. We show that α4β1 integrin promotes cell migration through both unconfined and confined spaces. However, unlike unconfined (2D) migration, which depends on enhanced Rac1 activity achieved by preventing α4/paxillin binding, confined migration requires myosin II-driven contractility, which is increased when Rac1 is inhibited by α4/paxillin binding. This Rac1-myosin II crosstalk mechanism also controls migration of fibroblast-like cells lacking α4β1 integrin, in which Rac1 and myosin II modulate unconfined and confined migration, respectively. We further demonstrate the distinct roles of myosin II isoforms, MIIA and MIIB, which are primarily required for confined and unconfined migration, respectively.

Protein kinase A (PKA) works upstream to regulate phosphorylation of verious proteins and enzymes, including α4β1 integrin. It has been reported that PKA tightly regulates wide array of (patho)physiological functions. We have further employed FRET-based-PKA reporter (AKAR4-Kras) to investigate how cells modulate PKA activity spatiotemporally. We have found that the interplay of PKA, Rac1/myosin II, and cytoskeleton-related molecules determines efficient migration in response to various degrees of physical constraint. This work provides a paradigm for the plasticity of cells migrating through different physical microenvironments.

Advisor:

Dr. Konstantinos Konstantopoulos

ACKNOWLEDGMENTS

First I need to thank Konstantinos Konstantopoulos for being a wonderful advisor. During my five year PhD lifetime, he ensures that I have sufficient freedom to develop my research. In many respects, he has always been very open-minded and financially supportive, which really enables many possibilities of my scientific development. I also need to thank him for allowing me to participate more than 8 grant and fellowship writing process, which sharps my scientific writing skill and also strengthens my resistance to pressure. I am honored, lucky, and perhaps destined to have him as my advisor.

Second I would like to thank Dr. Joy Yang for many things she has done for me. When I was first-year student with no any cell biology background, she is nice enough to take me, a stranger to her office for discussing many questions that I've brought. After that, we work very closely with my main project and she has always been very resourceful and helpful to my work. Her passion of chasing the truth of the science causes huge impact on me and I could have not come this far without her training.

Special thanks goes to Dr. Denis Wirtz. There is a meet-up on JHU shuttle bus and, again he nicely offers me a chance for discussion next day. In that meeting, he clearly pointed out my drawbacks, weakness of research, and advised many ways to improve my career and science. His words are like thunder striking to my mind and that short lessen became very useful for my research development. I also need to thank Dr. Jin Zhang for giving me the opportunity of initiating my last project in my late PhD. I also need to mention that the PhD student, Jessica Yang in Zhang's lab has been a wonderful partner to work with.

I need to thank all my previous and current labmates. I will especially appreciate Colin Paul, Jack Chen, and Kimberly Stroka for being so resourceful and for always providing very prompt help with my project. Tommy Tong has been a great big brother of lab, and his philosophy helped me quickly get used to lab environemnt. I also need to thank to Fei Zhu, and Wang Pu for providing so much mental and scientific supports when I was in the lowest in research. Finally I need to thank Zhizhan Gu for coming in my late PhD period. His experience and vision broaden my view, thus enabling me to better understand the realistic interplay of industry and academia.

Thanks Tom Shen from Gerecht lab, Wei-Chiang Chen, Anjil Giri, Meng Horng Lee, and Pei-Hsun Wu from Wirtz Lab for being such wonderful classmates and friends. They do not only provide scientific help in my research but also really fulfill my PhD life with cheerful out-class activities.

I also have special thanks to previous and current/prior academic administrators Sue Porterfield, Tracy Smith, and Caroline Qualls. Their help simplified complicated processes, which allows me focus on research itself without worry.

Finally, I need to thank all my family for encouraging me to pursue this degree in Johns Hopkins University. Without their words and support, I could not reach here.

Detachment from worldly desires polishes higher ideals; peaceful state of mind enables broader visions.

So one spares no effort in one's duty until the very end.

“澹泊以明志，寧靜以致遠”

TABLE OF CONTENTS

List of Figures

Figure description

CHAPTER 1

Introduction

Cell migration in different tissues occurs in variety of cell types. Migration is a constitutive feature for fibroblast, leukocytes, and different other kind of cells throughout lifetime. In general, cell migration plays critical role of maintaining various physiological function such as wound healing, leukocyte trafficking, gastrulation, and organ development. The mechanism of cell migration was first established on 2D migration. Cells are activated to perform multistep cycle of protrusion, adhesion formation, and stabilization at the leading edge followed by cell body translocation and release of adhesion and detachment of cell rear to complete movement. However, although 2D migration plays important role for heart or blood vessel development, migrating cells have high chance encountering various type of barrier and physical constraint in physiological development. Therefore simulating or modeling 3D migration has been developed to attempt to understand how cells migrate in vivo. The limitation of 3D migration is various factors such as control of local density, and growth factor stimulus and MMP-mediated ECM degradation could all physically or biochemically affect cell migration. In order to study basic mechanism of migration in response to physical constraint, we employed PDMS-based microchannel assay to simulate this process. Using CHO-α4WT as model system, we first study the effect of outside in signaling on confined migration. Moreover, we compared the mechanism of confined and unconfined migration in α4

expressing cancer cell line, melanoma, commonly used 3T3 fibroblast cell line, and T cells. With these comprehensive studies, we sought to reveal the mechanism of migration in response to physical constraint.

1.1 Role of integrins mediates cell migration (outside-in signaling)

Integrins are major and well-defined trans-membrane receptors that mediate dynamic interaction and extracellular matrix and the actin cytoskeleton during cell migration. Integrins recognize diverse specific ligands. For example, α5β1, αvβ3, and α4β1 integrins are specific to different regions of fibronection, α1β1 and α2β1 are specific to collagen, and α2β1, α3β1, and α6β1 integrins are specific to laminin. Cell surface receptor is also recognized by integrins, such as ICAM-1 (αLβ2) and VCAM-1 (α4β1). In order to migrate, integrin mediate adhesion assembly and reassembly by turning over, which optimize cell migration speed and persistence. The optimal migration speed happens when the interaction between integrin and substrate are intermediate where adhesion assembly and disassembly are efficient (Huttenlocher and Horwitz, 2011). It has been reported that α5β1 and α2β1 play important role of mediating this migration process and focal adhesion are mainly formed by these two integrin (Askari et al., 2010; Kreis et al., 2005). However, different integrins can also suppress the signaling from each other, given the best example that α4β1 integrin inhibits α5β1-indeuced stress fiber and focal adhesion (Moyano et al., 2003). Ligand-receptor binding not only provides physical anchor to cytoskeleton but also induces formation of adaptor protein complex in integrin cytoplasmic region, thus triggering signaling cascade that further modulates migration process.

α4β1-mediated 2D, confined, and 3D migration involves wide array of physiological process, including epicardium formation, T-cell trafficking, and melanoma metastasis. The α tail of α4β1 integrins also interacts with various

cytoskeletal proteins such as paxillin. These proteins, which directly associate with the tails of α4β1 integrin subunits, also interact with other proteins, forming an exquisitely regulated multiprotein complex that links to the actin cytoskeleton(Liu et al., 1999). In addition to their scaffolding function, these proteins transduce signals to regulate cell polarity, F-actin branching and polymerization and migration through a process known as "outside-in signaling", which is itself tightly regulated. Binding of paxillin to the α cytoplasmic domain has been reported to recruit protein complex ARF-GAP which then interferes with Rac1 activation at leading edge of the cell(Nishiya et al., 2005). Paxillin binding to α4 is prevented by phosphorylation of a critical serine residue (ser-988) in the α4 cytoplasmic tail. Upon dephosphorylation of α4 integrin, paxillin can bind to α4β1 integrin, which then results in their colocalization in focal complexes at the cell front and in focal contact at cell rear (Liu et al., 1999). Given that efficient integrin-dependent migration is achieved by Rac1-dependent lamellipodium induction and higher side integrin dynamics localizing at actin stress fibers upon RhoA activation, we know that paxillin binding and its prevention will modulate activities of Rac1 and RhoA, whose effects then result in different cell migration styles (Hung et al., 2013). Y991A is a α4 cytoplasmic point mutation prevents paxillin binding and, S988A is the point mutation preventing phosphorylation at serine residue of α4-tail. Previous research and we have together shown that CHO-α4Y991A cells exhibit wider lamellipodial protrusions (i.e. fan shape) and migrate in a more directionally persistent manner(Pinco et al., 2002). In contrast, CHO-α4S988A cells display confined lamellipodia protrusion and migrate less directionally(Goldfinger et al., 2003).

1.2 Conformation change of α4β1 integrin through inside-out signaling

α4β1 integrin is formed through non-covalent association of two type I

transmembrane glycoproteins, α4- and β1 subunit. The extracellular domains are approximately 700 amino acids for α- and 1000 amino acids for β subunits(Xiong et al., 2002). The globular head region of the extracellular domain of the α4 subunit participates in ligand binding by switching between close and open conformations. This α4 globular head region consists of seven repeats of 60 amino acids as well as an insertion termed I-domain that fold into a seven-bladed β propeller structure at inactivation state(Liddington and Ginsberg, 2002). This I-domain contains a "metal ion-dependent adhesion site" (MIDAS) and integrin ligand binding is altered by the coordination of Mg^{2+} ion and shifts from a closed to an open conformation. This process is thought to increase the binding affinity and the adhesion strength of α4β1 integrins. The β cytoplasmic tail has been reported to associate with various cytoskeletal and signaling proteins, such as talin, α-actinin, tensin, and focal adhesion kinase(Liddington and Ginsberg, 2002). Binding of talin to the β cytoplasmic tail of α4β1 induces integrin conformational changes that propagate all the way up to the ligand-binding head domain, thereby increasing α4β1 intergin affinity.

1.3 Using microfluidic device to study cell migration and invasion

Conventional transwell assay has been used for past decades. It used to be commonly used assay to measure cell motility and has been commercialized by several companies. However, it has several disadvantages such as that chemotaxis gradient varies over time and it is incapable of monitoring cell movement in real time. We have developed PDMS-based microchannel assay where stable gradient can last more than 15 hours and different degree of confinement can be created for the need of experiments(Tong et al., 2012a). Most importantly, this microschannel assay enables us to monitor cell morphological change during migration or invasion and it opens the possibility of integrating with other technologies, such as real time biosensor analysis.

Moreover, the array of microchannel provides a platform to quantify and identify the properties of cell migration. For example, microchannels can be either coated with specific substrate for migration study or filled in with matrigel for the purpose if invasion study (Chaw et al., 2007). Cell displays completely different migration phenotypes in both conditions. Within matrigel filled 6μm microchannel, chondrosarcoma exhibits mesenchymal phenotype where high MMP activity could be involved. In contrast, with collagen-I coated 6μm microchannel, cell migrates in a more amoeboid style where protrusion-retraction cycle is not found profound.

1.4 Overview of thesis

The focus of this study has been directed toward to reveal the mechanism of confined migration, and mechno-sensing. My efforts have been first concentrated with simulating a confined or 3D environment by employing microchannel migration assay, followed by series of Rac1-myosin II crosstalk study to reveal how fibroblast-like cells adjust signaling to optimize migration in response to physical constraint (Chapter 2 and Chapter 3). This study also demonstrates how myosin II isoforms can differentially regulate cell migration in confined and unconfined spaces in Chapter 4. Other than fibroblast-like cell lines, we also discovered both amoeboid artificial T-cell and in vivo T-cell use Rac1-myosin II balance to regulate confined versus unconfined migration, which is described in Chapter 5. Using FRET-based biosensor, Chapter 6 presents protein kinase A, which is upstream of α4 and many other factors, is locally modulated in response to physical confinement. We have summarized and discussed the biological significance, proposed signaling pathway of confined migration, and possible source of mechano-sensor in Chapter 7. Several suggested lines for future work are presented in Chapter 8.

CHAPTER 2

α4β1 integrin regulates confined versus unconfined migration

2.1 Introduction

Using a Chinese hamster ovary (CHO) cell model, it was demonstrated that α4β1 integrin promotes lamellipodia protrusion and directionally persistent cell migration, which are regulated by molecular interactions at the cytoplasmic tail of the α4 integrin subunit (α4 tail) (Goldfinger et al., 2003; Lim et al., 2007; Rivera Rosado et al., 2011). The best studied interaction at the α4 tail involves its binding to paxillin (Liu et al., 1999), which forms an α4-paxillin-GIT1 complex that inhibits Rac1 activation (Nishiya et al., 2005). α4/paxillin binding is negatively regulated by PKA-dependent phosphorylation of Ser988 in the α4 tail (Ser^{988}-phosphorylation) (Han et al., 2001). α4β1 integrin-dependent cell migration on a two-dimensional (2D) substratum is suppressed when Ser^{988}-phosphorylation is disrupted by substitution of Ser988 with Ala (S988A mutation) but enhanced when α4/paxillin binding is disrupted by substitution of Tyr991 with Ala (Y991A mutation). α4/paxillin binding and Ser^{988}-phosphorylation differentially modulate Rac1 activation, thus regulating lamellipodia protrusion and directionally persistent cell migration on a 2D surface (Goldfinger et al., 2003; Nishiya et al., 2005). However, it is not known how the molecular interactions at the α4 tail regulate cell migration through physically confined, as opposed to unconfined (2D), microenvironments encountered *in vivo*.

Cells migrate *in vivo* within 3D ECMs. Cells also migrate through 3D longitudinal tracks with bordering 2D interfaces (i.e. channels). These channels are formed between the connective tissue and the basement membrane of muscle, nerve and epithelium (Friedl and Alexander, 2011). 3D longitudinal channels are also formed between adjacent bundled collagen fibers in fibrillar interstitial tissues (Friedl and Alexander, 2011). Importantly, cells have been reported to migrate through such 3D channels *in vivo* (Alexander et al., 2008). The cross-sectional areas (Wolf et al., 2009) of pores/channels encountered *in vivo* range from 10 to >400 μm^2. Consequently, cells migrating *in vivo* experience varying degrees of physical confinement. Accumulating evidence suggests that physical confinement alters cell migration mechanisms (Balzer et al., 2012; Konstantopoulos et al., 2013; Pathak and Kumar, 2012). To address how α4 tail-mediated signaling regulates cell migration in physically confined microenvironments, we used a microchannel device (Balzer et al., 2012; Chen et al., 2013; Tong et al., 2012a), which tracks cells migrating through 4-walled channels of varying degrees of confinement; from unconfined (2D) migration when the channel width, W, is larger than the cell diameter, d_{cell}, (wide channels) to confined migration when $W<d_{cell}$ (narrow channels).

2.2 Materials & Methods

2.2.1 cell culture

CHO-α4WT, CHO-α4Y991A, or CHO-α4S988A cell lines were generated by stably transfecting CHO cells with pQN4G, pQN4Y991AG or pQN4S988AG plasmids, in which wild-type or mutant α4 integrin cDNA was inserted into a

PGBI25-fN1 GFP vector (Dikeman et al., 2008; Pinco et al., 2002). The cells were maintained in Ham's F12 (Cellgro, 10-080-CM, company) medium.

2.2.2 flow cytometry

Flow cytometry, immunoprecipitation, and immunoblot analysis were performed as described by Pinco et al.(Pinco et al., 2002) For flow cytometry, an anti-α4-integrin antibody (clone P1H4 from Millipore-Chemicon) and a goat anti-mouse allophycocyanin-conjugated secondary antibody (Santa Cruz Biotechnology) were used.

2.2.3 microfluidic-based microchannel assay

PDMS microchannels were fabricated using standard replica molding. Masks to generate the microchannel design were drawn using Adobe Illustrator CS2 and printed onto a transparency by a 5080 dpi printer (Pageworks) or transferred to a chrome-on-glass photolithography mask (Advance Reproductions Corp.). To prepare masters, SU-8 2010 and SU-8 2025 epoxy negative photoresists (Microchem Corp.) were applied by spin coating (Laurell Technologies Corp.) onto silicon wafers (Montco Silicon Technologies Inc.) in two steps. SU-8 2010 was first spread at 600 rpm for 20 s and then at 4000 rpm for 60 s to a final thickness of 8-10 μm. The photoresist was prebaked at 60 °C for 1 min, exposed to UV (350−450 nm) radiation through appropriate masks for 40 s, postbaked at 115 °C for 8 min, and subsequently developed using SU-8 developer (Microchem Corp.). This step was used for generating the microchannels present in the final device. The second feature of the microfluidic-based microchannel master consisted of the cell seeding line and the FBS gradient generation line, and was fabricated using the following steps: SU-8

2025 was first spread at 500 rpm for 10 s and then at 4000 rpm for 30 s to a final thickness of 50 μm. The photoresist was prebaked at 80 °C for 3 min and at 110 °C for 6 min, cooled, and exposed to UV (350−450 nm) radiation for 30 s through a mask aligned with the previously fabricated microchannels. The photoresist was then exposed for 8 min at 110 °C and developed as before. PDMS stamps were obtained by mixing Sylgard 184 prepolymer with cross-linker (Dow Corning) in a 10:1 ratio (by weight), degassing in a vacuum, and curing at 80 °C for 1 h. Each PDMS well inlet and outlet was punched out with a diameter of 6 mm. Both the PDMS device and microscope slide (FisherFinest) were cleaned and made hydrophilic using a plasma cleaner for 2 min. The PDMS device was then attached to a glass slide, followed by pre-coating various concentrations of VCAM-1 at 37 °C for 1 h. The microchannel was washed with PBS (1X) containing calcium/magnesium for 1 min before seeding cells. A total of $1x10^5$ cells in a 50 μl volume were added to the cell inlet port. Chemotactic-driven cell migration was recorded via time-lapse microscopy (inverted Eclipse Ti microscope, Nikon) using software controlled stage automation (Nikon). To calculate migration velocity, the cell center was identified as the midpoint between poles of the cell body, and was tracked for changes in X, Y position at 20-min intervals or 5-min intervals only for $CD4^+$ T cells over a 10 h period.

2.3 Results & Discussion

2.3.1 overview of using microchannel assay on CHO cells expressing α4

To study the effects of α4 cytoplasmic tail interactions on cell migration, we used stable CHO cell lines, which ectopically express the wild-type α4 integrin (CHO-α4WT) or α4 integrin carrying specific cytoplasmic mutations that disrupt paxillin binding (CHO-α4Y991A) or Ser^{988}-phosphorylation (CHO-α4S988A)

(Dikeman et al., 2008; Pinco et al., 2002). We confirmed that CHO-α4WT, CHO-α4Y991A and CHO-α4S988A cells express equivalent levels of α4 integrin on their surface, as assessed by flow cytometry (**Fig. 2-1**). We tested the migratory potential of each cell type in a microchannel assay (Balzer et al., 2012; Chen et al., 2013; Tong et al., 2012a). In this assay, cells migrate toward a chemoattractant source through VCAM-1- or fibronectin-coated, 4-walled rectangular channels of fixed length (200 μm) and height (10 μm) but variable width (3, 6, 10, 20 or 50 μm) (**Fig. 1**). Cells migrating through 50-μm wide channels are not constricted by the PDMS channel walls and protrude lamellipodia similar to those on 2D planar surfaces (**Figs. 2-1, 2-2**).

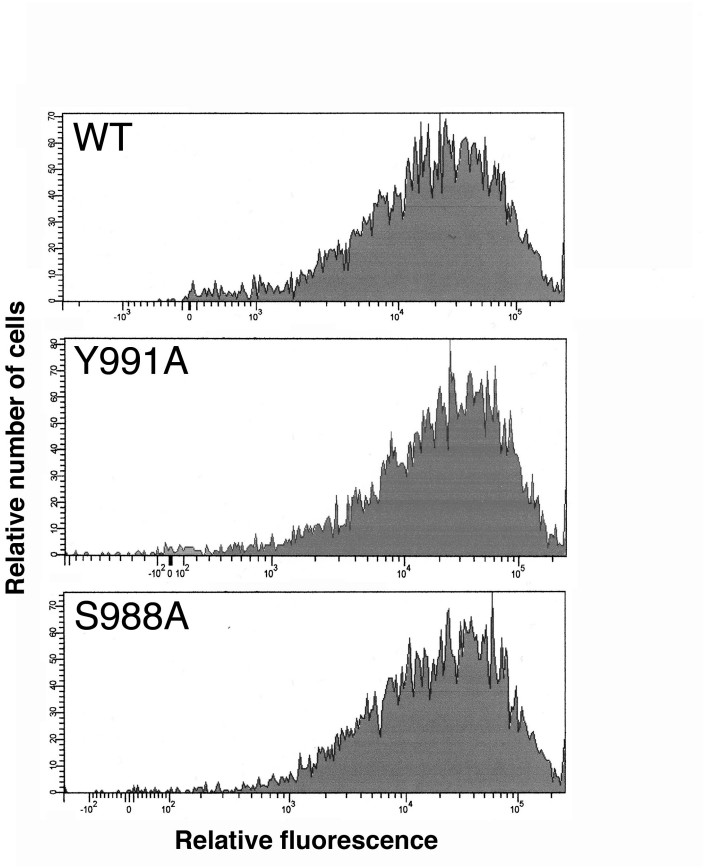

Figure 2-1 α4 expressing level of CHO-α4WT, CHO-α4Y991A and CHO-α4S988A cells. Demonstrates surface expression of α4 integrin in CHO-α4WT, CHO-α4Y991A and CHO-α4S988A cells. Fig. S2 details quantitative analysis of velocity, speed and chemotactic index of α4 integrin-expressing CHO, A375-SM and Jurkat T cells in wide and narrow channels.

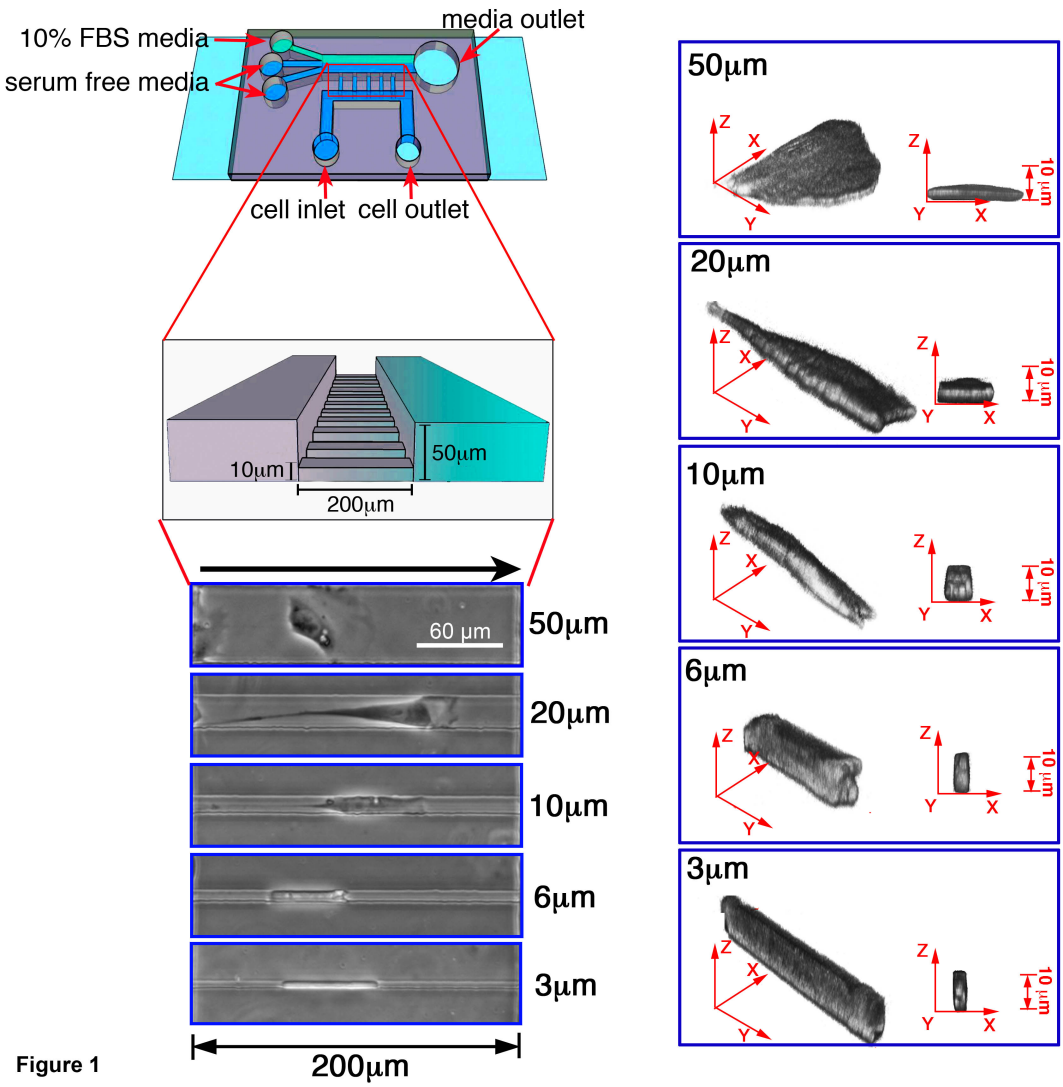

Figure 1

Figure 2-2 Overview of the microchannel device. Schematic of the migration chamber bonded to coverslips (light blue), with inlet ports for serum-free media or cells (dark blue) or FBS (10%; green). Also shown is a close-up detailing the dimensions of the microchannel array, along with phase contrast and 3D reconstruction images of CHO-α4WT cells in microchannels of different widths. The black arrow (above the phase images) indicates the direction of migration.

2.3.2 α4 tail mutations exert distinct effects on wide versus narrow channel migration

We then evaluated the effect of VCAM-1 concentration on the speed of cell migration. As shown in **Fig. 2-3 A**, all cell types migrating through 50-μm wide channels exhibited a biphasic dependence of the migration speed on ligand concentration, with maximum speeds at intermediate VCAM-1 concentrations (1-2 μg/ml corresponding to ~1150-2000 molecules/μm^2, as determined by the Europium assay (Tong et al., 2012b)). This pattern is typical of 2D migration (DiMilla et al., 1993). Consistent with previous reports (Goldfinger et al., 2003), CHO-α4S988A cells displayed the lowest migration speed over a wide spectrum of ligand concentrations, whereas CHO-α4Y991A cells had either a similar migration speed with CHO-α4WT cells at low/intermediate VCAM-1 concentrations or moved faster than CHO-α4WT at higher ligand concentration (≥5 μg/ml) (**Fig. 2-3 A**).

As the channel width decreases (W<50 μm), cells progressively experience physical confinement by the lateral channel walls, and undergo deformation to squeeze and move through the channels (**Fig. 2-2**). Narrow (6 or 3 μm) channels induce cell contact with all 4 channel walls, and emulate migration through a physically constricted microenvironment (referred to as confined migration) (Balzer et al., 2012). In narrow channels, the migration speed of CHO-α4WT cells remained maximal up to intermediate VCAM-1 concentrations (0-2 μg/ml), and progressively decreased at higher concentrations (**Fig. 2-3A**). In contrast to wide (50 μm) channels, CHO-α4Y991A cells exhibited the lowest migration speed over a wide range of VCAM-1 concentrations, whereas CHO-α4S988A migrated as efficiently as CHO-α4WT cells at low/intermediate VCAM-1 concentrations in narrow channels (**Fig. 2-3A**). We also quantified migration persistence by measuring the cell chemotactic

index (defined as the ratio of the net displacement to the total distance traveled) and migration velocity (defined as net displacement divided by time). No major differences were noted between migration speed versus velocity because all CHO cell types had persistent cell motility in response to FBS **(Figs. 2-3A)**. Because migration velocity represents the overall motile activity of the cells in response to a chemotactic stimulus, this parameter was used in the studies hereafter.

We quantified the migratory velocity of each cell type in response to increasing degrees of confinement using microchannels coated with 1 μg/ml VCAM-1, because this concentration provided near maximal speeds of migration in both wide and narrow channels. CHO-α4WT cells migrated efficiently through channels of different widths with a migration velocity of ~30 μm/h. CHO-α4Y991A cells displayed progressively reduced cell motility in channels of decreasing width (**Fig. 2-3B**). In contrast, the velocity of CHO-α4S988A cells gradually increased with decreasing channel width (**Fig. 2-3B**). Similar phenomena were also observed in fibronectin-coated (5 μg/ml) microchannels (**Fig. 2-3C**), thereby generalizing our observations to ECM proteins found in confined spaces *in vivo*. These data reveal the divergent effects of the α4 tail mutations on the migration of α4β1 integrin-expressing CHO cells through wide versus narrow channels. They also suggest that α4β1 integrin may modulate and optimize cell migration via distinct mechanisms when the cells are subjected to different physical microenvironments.

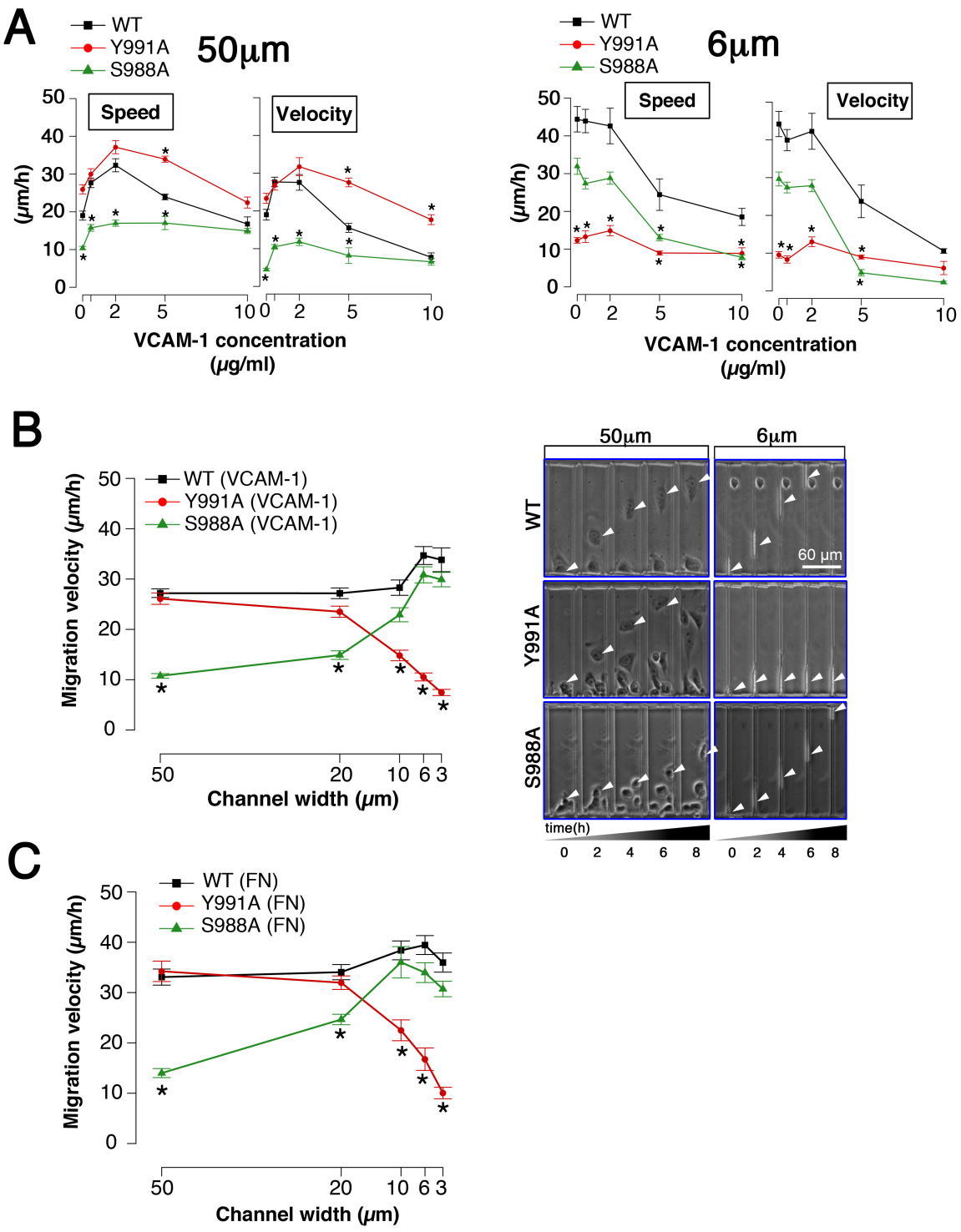

Figure 2-3 Effects of the α4-tail mutations on cell migration in microchannels.

(A) The migration speed and velocity of CHO-α4WT, CHO-α4Y991A and CHO-α4S988A cells through 50-μm or 6-μm microchannels as a function of VCAM-1 coating concentration. Data represent mean ± SEM of >20 cells from 3 independent

experiments. **(B-C)** The influence of channel width on cell migration velocity through microchannels coated with 1 μg/ml VCAM-1 (B) or 5 μg/ml fibronectin (C). Data represent mean ± SEM of >30 cells from 3 independent experiments. In (B), the images of migrating cells in designated channel widths and time-points are also shown. White arrowheads, the centroid of cell body. Bar, 60 μm. For all panels, *, P <0.005 relative to CHO-α4WT.

CHAPTER 3

α4β1 integrin regulates Rac1/myosin II crosstalk pathway

3.1 Introduction

Nowadays Rho family can be categorized into five groups, Rho-like, Rac-like, Cdc42-like, Rnd, and RhoBTB subfamilies. Rac-like families are responsible of stimulating lamellipodia and membrane ruffles. Lamellipodia are the protrusive structures generated at the leading edge of migrating cells. Previous finding shows that Rac1 can play the role of activating WAVE to stimulate Arp2/3 to nucleate actin polymerization(Pollard, 2007). This pathway facilitates net-like actin polymerization and promotes protrusion activity of leading protrusion. Rho-like families are playing he roles of inducing stress fiber and focal adhesion formation. The Rho effector, Rho-kinase can directly activate myosin II light chain or through inhibiting myosin light chain phosphatase (Gallo, 2006; Wang et al., 2009b), therefore enhancing myosin II contractility.

The crosstalk between Rho families has always been the focus of cell migration study. Activation of Rac has been proved to cause the inactivation of Rho and vise versa(Newell-Litwa and Horwitz, 2011). One of negative feedbacks from Rac1 to RhoA can be due to the activated p190RhoGAP(Arthur and Burridge, 2001). Moreover it has reported that PAK, the Rac effector can also play the role of inhibiting RhoA activity (Li et al., 2011). In the other hand, the high myosin II activity can suppress Rac1 activation (Hung et al., 2013; Lee et al., 2010).

In Chapter 2, we have already described the migration phenotypes of CHO-α4Y991A cells, where α4/paxillin binding mutation promotes Rac1-driven protrusion of leading edge and CHO-α4S988A cells, where α4 phosphorylation mutation prevent local Rac1 activation. We speculate the α4 signaling can modulate Rac1/myosin II balance in different physical constraint, thus playing important role of regulating cell migration in response to different physical confinement. In this chapter, we employ immuno-fluorescence, bio-molecular method, and Rac1 biosensor, combining with microchannel assay to investigate how α4-expressing or non-α4 expressing cells optimize the migration in different degree of confinement by modulating Rac1/myosin II signaling balance.

3.2 Materials & Methods

3.2.1 cell culture, pharmacological inhibitors, plasmid and transfection

Methods of maintaining α4 expressing-CHO cells were described in Chapter 2. CHO cells, 3T3 fibroblasts and A375-SM cells were maintained in DMEM (high glucose, Life technology). Media were supplemented with 10% fetal bovine serum (FBS, Gibco) and 1 μg/ml penicillin/streptomycin. For inhibitor studies using fibroblast-like cells, 100 μM NSC23766 (Calbiochem), 25 μM ML-7 (Sigma), 45 μM Y-27632 (Sigma), 50 μM blebbistatin (Cayman), 22.5 μM 6B345BBQ (Sigma) or appropriate vehicle controls were added to the cells seeded in serum-free medium near microchannel entrances. Jurkat T cells and primary $CD4^+$ cells were treated with 20 μM NSC23766, 75 μM blebbistatin, 90 μM 6B345TTQ or appropriate vehicle controls. For antibody blocking experiments, cells were treated with 3 μg/ml of anti-α4 integrin mAb (clone P1H4, Millipore). After 1 h of incubation with the inhibitors or antibody at 37 ^oC, the chemoattractant (10% FBS) was added to topmost inlet port

(**Fig. 2-2**) to induce cell migration. Rac1-siRNA, ROCK-siRNA and control siRNA were from Santa Cruz Biotechnology. The RFP-PAK-PDB (in a modified pUW vector) was a gift from Peter Devreotes (JHU, Baltimore, MD). Transient transfection was performed using Lipofectamine 2000 (Life Technologies) according to the manufacturer's protocol.

3.2.2 Stress fiber imaging and quantification

Cells were either plated on coverslips overnight or induced to migrate through channels of prescribed widths coated with 1 μg/ml VCAM-1. The cells were then fixed with 3.7% formaldehyde for 10 min, followed by permeabilization with 0.1% Triton X-100 for 10 min, and a 30 min blocking at room temperature (RT) with 1% BSA. After washing 3X with PBS, cells were incubated with Alexa568-conjugated phalloidin (1:500; Molecular Probes) for 1 h at RT. Images were captured at 12-bit depth on a Zeiss Axiovert 200 LM (Carl Zeiss) equipped with an LSM 510 META laser confocal scanner and a 63X/1.4 NA oil-immersion objective. For all acquisitions, detector voltage, scan speed, pixel resolution, laser power and optical zoom were standardized and utilized consistently to ensure quantitative image analysis. Captured images were exported as raw uncompressed TIFF images. Images of phalloidin-stained cells were processed using the following steps to extract the values of stress fiber density in ImageJ: (a) enhance intensity using default setting, (b) subtract the background, and (c) convert the processed image to black-and-white using the binary setting in ImageJ. Stress fiber area was identified as the pixels with value 255, distinguished from others pixels with value zero. Lastly, (d) stress fiber density was calculated as the percentage total cell spreading area occupied by stress fiber area. To obtain 3D images of actin in various degrees of confinement, the 3D viewer in ImageJ was used to reconstruct serial z-planes into a 3D rendering.

3.2.3 Focal adhesion imaging and quantification

Cells were plated on VCAM-1-coated coverslips and allowed to spread for ~16 h, then fixed in 3.7% formaldehyde for 10 min, permeabilized in 0.5% Triton-X 100 for 5 min, and blocked in 2.5% BSA for 1 h. Cells were immunostained using an antibody against pY-paxillin (Cell Signaling) at 1:100 dilution for 2 h, followed by an Alexa 568 secondary antibody (Invitrogen) at 1:100 dilution for 1 h. Cells were washed 3 times with PBS in between each step and all steps were completed at RT. The stained cells were imaged by total internal reflection fluorescence (TIRF) microscopy using an inverted 3i Marianas microscope equipped with dual Photometrics Cascade II 512 EMCCD cameras for simultaneous 2-channel TIRF acquisition, along with a 100x/NA 1.45 oil immersion lens and Slidebook 8.0 software. TIRF images were processed and quantified as previously described (Stroka and Aranda-Espinoza, 2011; Stroka et al., 2012). Briefly, images were made binary and the particle analyzer tool was used in ImageJ to measure PY-paxillin-positive punctate areas larger than 0.1 μm^2, total focal adhesion area, or number of focal adhesions per area. Total cell area for each image was determined by tracing α4-GFP-positive areas on TIRF images. TIRF experiments were repeated 3 times, for a total of 40-60 cells per condition.

3.2.4 Rac1 activity measurement by ELISA

Cells were transfected with 1 ng/ml RFP-PAK-PDB. After 48 h of transfection, the cells were treated with the designated inhibitors or appropriated vehicle controls. Live images were taken by either broad field (inverted Eclipse Ti microscope, Nikon) or confocal (Zeiss Axiovert 200 LM as described above) dual-color fluorescent microscopy. The activated Rac1 level was quantified by averaging TRITC intensity normalized by averaged FITC intensity of the cells. For the α4 integrin-expressing

CHO cells, the FITC intensity was extracted from expression of GFP-tagged α4 integrin. For A375, 3T3 and CHO cells, FITC intensity was extracted from background.

3.2.5 Rac 1 activity measurement using a Rac1 probe

The Rac1 activity was measured using the G-LISA Rac Activation Assay kit (Cytoskeleton). In brief, CHO-α4WT, CHO-α4Y991A, or CHO-α4S988A cells were plated on 1μg/ml VCAM-1 for 12 h, in the presence of select inhibitors or appropriate vehicle control. Cell lysates were then prepared and incubated on Rac-GTP affinity plates, followed by incubation with an anti-Rac1 antibody. The signal was determined by measuring absorbance at 600 nm using a microplate reader

3.3 Results & Discussion

3.3.1 Inhibition of Rac1 activation and the RhoA-myosin pathway in CHO-α4WT cells recapitulate the migratory phenotypes of CHO-α4S988A and CHO-α4Y991A cells, respectively

The finding that α4/paxillin binding inhibits Rac1 activation (Nishiya et al., 2005) prompted us to investigate the role of Rac1 in cell migration through channels of varying degrees of confinement, using the Rac1-specific small molecule inhibitor NSC23766 (100 μM). CHO-α4WT cells treated with NSC23766 displayed reduced lamellipodial protrusion relative to controls and a markedly suppressed migration velocity through 50-μm wide channels (**Fig. 3-1A**). The inhibitory effect of NSC23766 was progressively diminished with decreasing channel width, and was minimal for the migration of CHO-α4WT cells through 10-, 6- or 3- μm channels (**Fig. 3-1A**). To confirm the specificity of this intervention, we knocked down Rac1 in CHO-α4WT cells via RNAi, and examined the migratory potential of Rac1-depleted

and scramble control cells in the microchannel assay. The efficacy of Rac1 depletion was verified by immunoblotting (**Fig. 3-1A**). Our data reveal that Rac1 knockdown repressed cell migration in wide, but not narrow, channels (**Fig. 3-1A**). Thus, inhibition of Rac1 activation in CHO-α4WT cells recapitulates the migratory phenotype of CHO-α4S988A cells in the microchannel assay. Because Rac1 can down-regulate myosin II via inhibition of RhoA-associated protein kinase (ROCK) or other mechanisms (Burridge and Wennerberg, 2004; Guilluy et al., 2011), we also tested the effects of the ROCK inhibitor Y-27632 (Liao et al., 2007) and myosin II ATPase cycle inhibitor blebbistatin (Limouze et al., 2004) on the migration velocity of CHO-α4-WT cells. In 50-μm channels, CHO-α4WT cells treated with Y-27632 (45 μM) or blebbistatin (50 μM) displayed an abnormal migratory morphology similar to that reported by (Even-Ram et al., 2007); the trailing edge failed to retract to the cell body and formed a long tailed structure (**Fig. 3-1A**), while the leading edge exhibited increased lamellipodia protrusion. Neither Y-27632 nor blebbistatin significantly altered the migration velocity of CHO-α4WT cells in 50-, 20- or 10-μm channels. In contrast, these agents effectively suppressed CHO-α4WT cell migration in narrow (6- and 3-μm) channels relative to controls (**Fig. 3-1A)**. Notably, ROCK1-depleted CHO-α4WT cells displayed a similar migratory phenotype to Y-27632- or blebbistatin-treated CHO-α4WT cells (**Fig. 3-2B**). Thus, inhibition of the RhoA-myosin II pathway in CHO-α4WT cells recapitulates the migratory phenotype of CHO-α4Y991A cells in the microchannel assay.

These data show that the migration velocity of the α4β1 integrin-expressing CHO cells is modulated and optimized predominantly by Rac1 in wide channels, whereas the myosin II pathway attunes migration in narrow channels. While the S988A mutation may suppress wide channel migration by inhibiting Rac1 activation

(Goldfinger et al., 2003; Nishiya et al., 2005), we hypothesize that Y991A may repress narrow channel migration by enhancing Rac1 activity, which in turn negatively regulates myosin II contractility through a crosstalk mechanism.

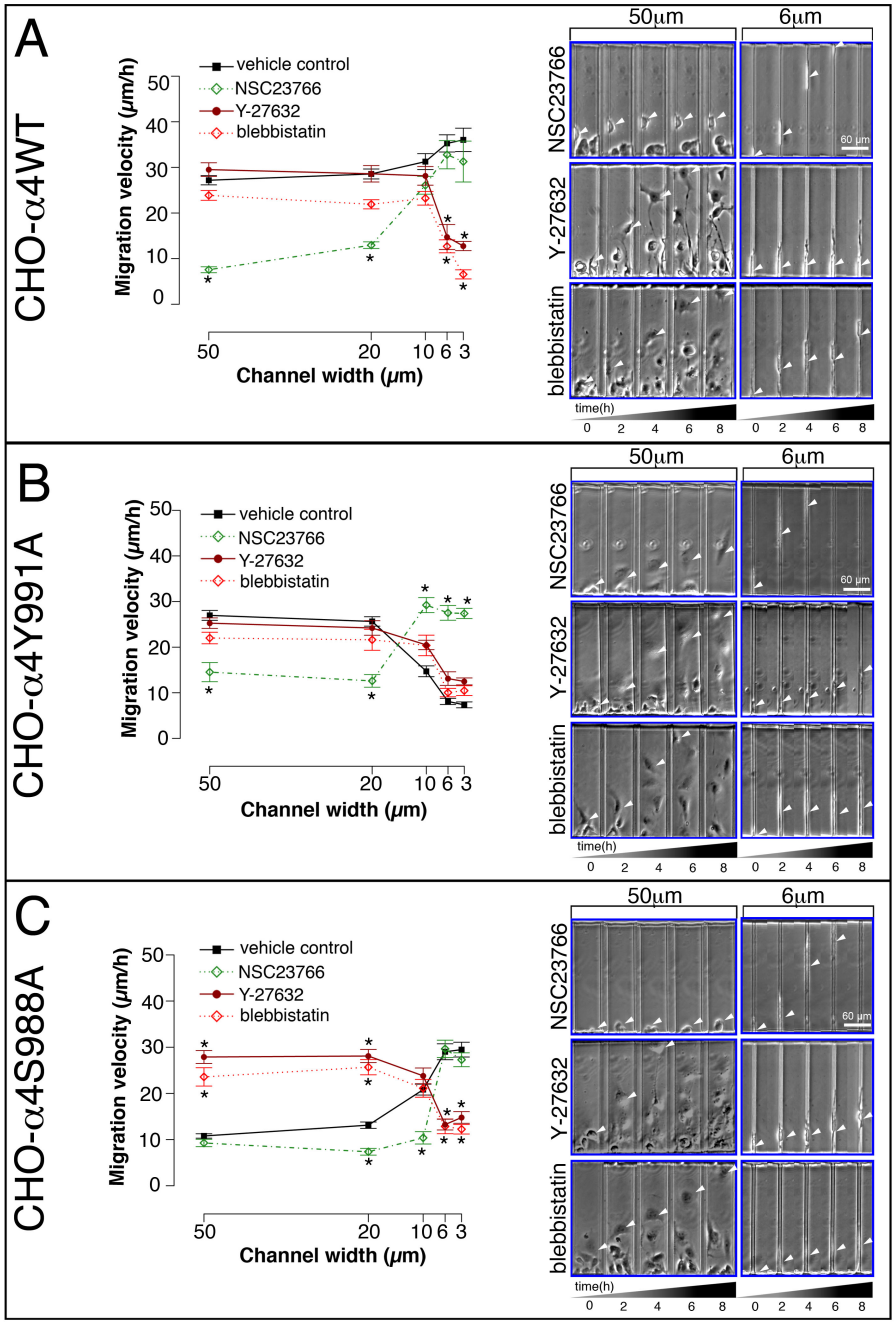

Figure 3-1 Effects of inhibiting Rac1, ROCK or myosin II on the migration of CHO-α4WT, CHO-α4Y991A, CHO-α4S988A cells in microchannels. (A) CHO-α4WT, **(B)** CHO-α4Y991A, and **(C)** CHO-α4S988A cells were treated with either the Rac1 inhibitor NSC23766, the ROCK inhibitor Y-27632, the myosin II inhibitor blebbistatin or vehicle control, and allowed to migrate inside VCAM-1-coated channels. Their migration velocities in channels of different widths were quantified.

Data represent mean ± SEM of >40 cells from 3 independent experiments. *, P <0.005 relative to control. The images of migrating cells in designated channel widths and time-points are also shown. White arrowheads, the centroid of cell body. Bar, 60 μm.

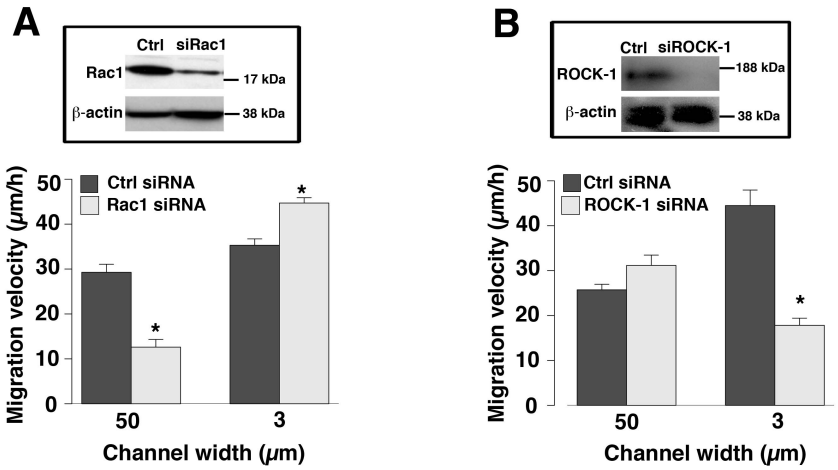

Figure 3-2 . Effects of Rac1 and ROCK-1-depletion on the migration of CHO-α4YWT cells. CHO-α4WT cells were transfected with Rac1 siRNA (30 nM) **(A)**, or ROCK-1 siRNA (200 nM) **(B)** or control siRNA (Ctrl) at the corresponding concentrations. The depletion of Rac1 and ROCK-1 was demonstrated by immunoblotting using an anti-Rac1 and anti-ROCK-1 antibody, respectively. β-actin served as an internal control. The migration velocity of Rac1-, ROCK-1- depleted or control CHO-α4WT cells inside 50-μm and 3-μm channels was quantified. Data represent mean ± SEM of >45 cells from 3 independent experiments. *, $P < 0.005$ relative to a control siRNA.

3.3.2 α4/paxillin binding regulates narrow channel migration through a crosstalk between Rac1 and myosin II.

To test this hypothesis, we first examined if attenuation of Rac1 activity in CHO-α4Y991A cells alleviates the inhibitory effect of the Y991A mutation on α4β1-regulated narrow channel migration. Indeed, the treatment of CHO-α4Y991A cells with the Rac1 inhibitor NSC23766 greatly enhanced narrow channel migration (**Fig. 3-1B**). As expected, this intervention suppressed wide (50- and 20-μm) channel migration of CHO-α4Y991A cells (**Fig. 3-1B**). In line with prior observations showing that S988A mutation inhibits Rac1 activation (Goldfinger et al., 2003; Nishiya et al., 2005), NSC23766 treatment had little effect on the migration velocity of CHO-α4S988A cells through either wide (50-μm) or narrow (6- or 3-μm) channels compared to controls (**Fig. 3-1C**). In contrast to NSC23766, Y27632 and blebbistatin did not affect the migration of CHO-α4Y991A cells through wide or narrow channels (**Fig. 3-1B**), but reversed the migratory phenotype of CHO-α4S988A cells, by markedly enhancing wide channel migration and suppressing narrow channel migration (**Fig. 3-1C**). Therefore, suppression of narrow channel migration by Y991A mutation can be rescued by inhibiting Rac1, whereas suppression of wide channel migration by S988A can be rescued by inhibiting the myosin II pathway.

3.3.3 Using PAK-PBD probe and ELISA assay, stress fiber and focal adhesion quantification to verify Rac1-myosin II crosstalk in molecular level.

We next asked if treatment with the Rac1 inhibitor NSC23766 enhanced myosin II activity in CHO-α4Y991A cells. Because the assembly of stress fibers depends on the contractile activities of myosin II, quantifying the formation of stress fibers is a valid measure of myosin II-driven contractility (Chrzanowska-Wodnicka and Burridge, 1996). Furthermore, tyrosine-phosphorylation of paxillin (PY-paxillin) in

focal adhesions depends on myosin II activity (Pasapera et al., 2010) and can also be used to evaluate cell contractile activity. When plated on VCAM-1-coated glass coverslips, CHO-α4S988A cells had the highest densities of stress fibers (**Fig. 3-3A-C**) and PY-paxillin-positive focal adhesions (**Fig. 3-3D-F**), whereas CHO-α4Y991A cells had the lowest. Notably, the stress fiber and focal adhesion defects in CHO-α4Y991A cells were rescued when the cells were treated with the Rac1 inhibitor NSC23766 (**Figs. 3-3 Ae, C and 3-3 Dd, F**). On the other hand, the NSC23766 treatment did not have any significant effect on the stress fiber density of either CHO-α4WT or CHO-α4S988A cells. To confirm that the changes in stress fiber density reflect altered myosin II activity, we showed that blebbistatin significantly suppressed stress fiber density in CHO-α4WT and CHO-α4S988A cells (**Fig. 3-3 A g, i, C**). Moreover, blebbistatin also dramatically reduced the density of PY-paxillin-positive focal adhesion in CHO-α4S988A cells (**Fig. 3-3 De, F**). However, blebbistatin failed to significantly suppress the already low stress fiber density of CHO-α4Y991A cells (**Fig. 3-3C**). Similar stress fiber phenotypes were observed when the cells migrated inside 6-μm channels **(Fig. 3-4)**. Under this confined condition, CHO-α4WT and CHO-α4S988A cells formed arrays of stress fibers that were aligned parallel to the channels (**Fig. 3-4 a, c**). In contrast, stress fibers were not detected in CHO-α4Y991A, but this stress fiber defect was rescued by treating cells with NSC23766 (**Fig. 3-4 b, e**). Blebbistatin treatment, as expected, diminished stress fibers (**Fig. 3-4 g-i**). Therefore, myosin II activity is reduced when α4/paxillin binding is disrupted by Y991A, and this can be rescued by Rac1 inhibition. We conclude that α4/paxillin binding promotes narrow channel migration by maintaining a high level of myosin II activity via its negative effect on Rac1.

We also quantified the activity of Rac1 in CHO-α4WT, CHO-α4Y991A and CHO-α4S988A cells using a PAK-PBD fluorescent probe (**Fig. 3-5A, B**) or ELISA (**Fig. 3-5C**). In both assays, Rac1 activity was the highest in CHO-α4Y991A cells, and it was inhibited by NSC23766. In contrast, Rac1 activity was the lowest in CHO-α4S988A cells. Notably, it was markedly increased by blebbistatin, thereby revealing that the inhibitory effect of the α4S988A mutation on Rac1 and the concomitant migration defect in wide channels can be rescued by a negative feedback of myosin II to Rac1.

Taken together, our data show that CHO-α4WT cells can migrate efficiently in both wide and narrow channels, but through distinct mechanisms. In wide channels, a high level of Rac1 activity is maintained in cells when myosin II activity is low and the binding between α4 integrin and paxillin is suppressed by Ser^{988}-phosphorylation at the α4 tail. This allows efficient cell migration in wide channels. In contrast, in narrow channels myosin II activity is enhanced by α4/paxillin binding through Rac1 inhibition, which promotes efficient migration in narrow channels. Both wide and narrow channel migration involve Rac1-myosin II crosstalk.

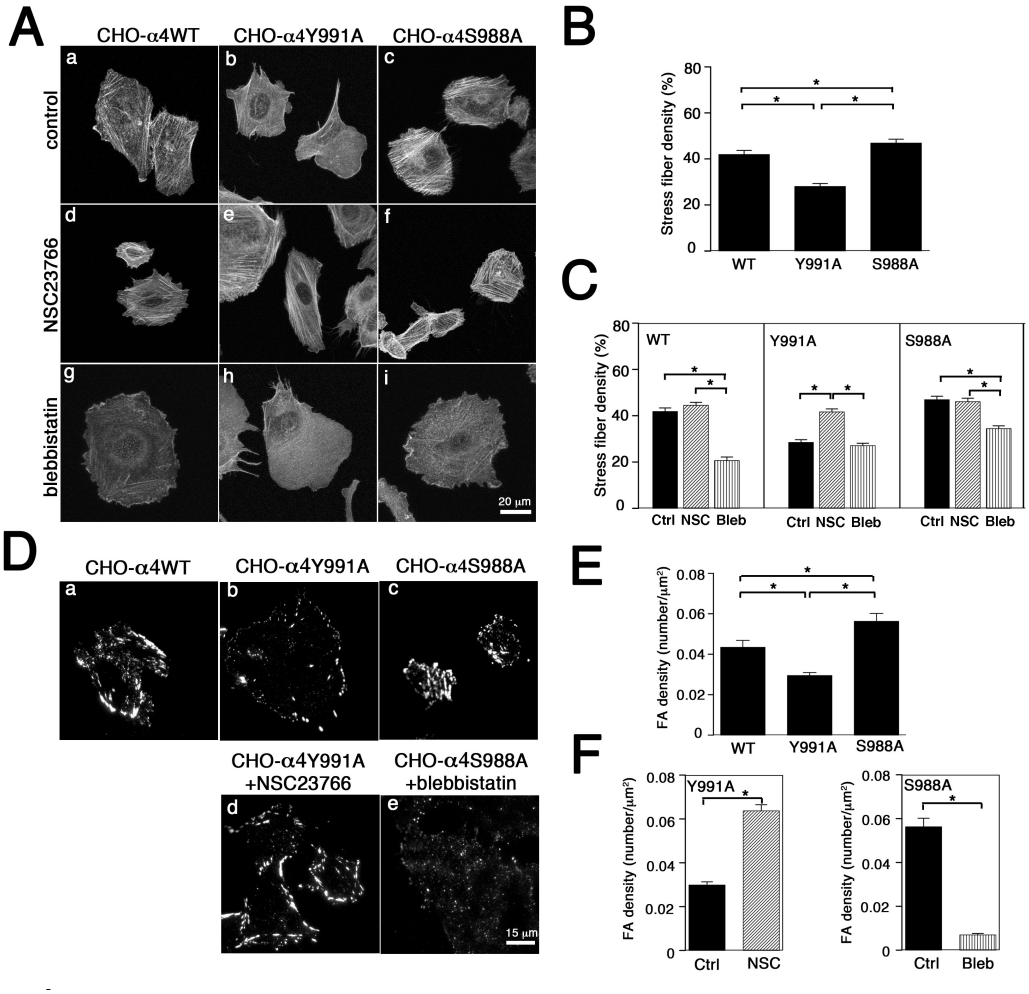

Figure 3-3 Effects of inhibiting Rac1 or myosin II on stress fiber and focal adhesion densities in cells migrating on 2D surfaces. CHO-α4WT, CHO-α4Y991A or CHO-α4S988A cells were plated on VCAM-1-coated coverslips in the presence of vehicle control **(A*a-c,* D*a-c*)**, NSC23766 **(A*d-f,* D*d*)** or blebbistatin **(A*g-i*, D*e*)**. **(A)** Cells were stained with TRITC-conjugated phalloidin and imaged by confocal microscopy. **(B-C)** Stress fiber density was measured and graphed as percentage total cell area occupied by stress fibers in the absence **(B)** or presence of NSC23766 (NSC) or blebbistatin (Bleb) **(C)**. Data represent mean ± SEM of 40 cells from 3 independent experiments. *, P <0.05 relative to control. (**D)** Cells were stained with an antibody against pY-paxillin and imaged by TIRF microscopy. **(E-F)** Focal adhesion density

was measured as the number of focal adhesions per μm^2 in the absence **(E)** or presence of NSC23766 (NSC) for CHO-α4Y991A or blebbistatin (Bleb) for CHO-α4S988A cells **(F)**. Data represent mean ± SEM of 45 cells from 3 independent experiments. *, $P < 0.05$ relative to control. Bar, 20 μm.

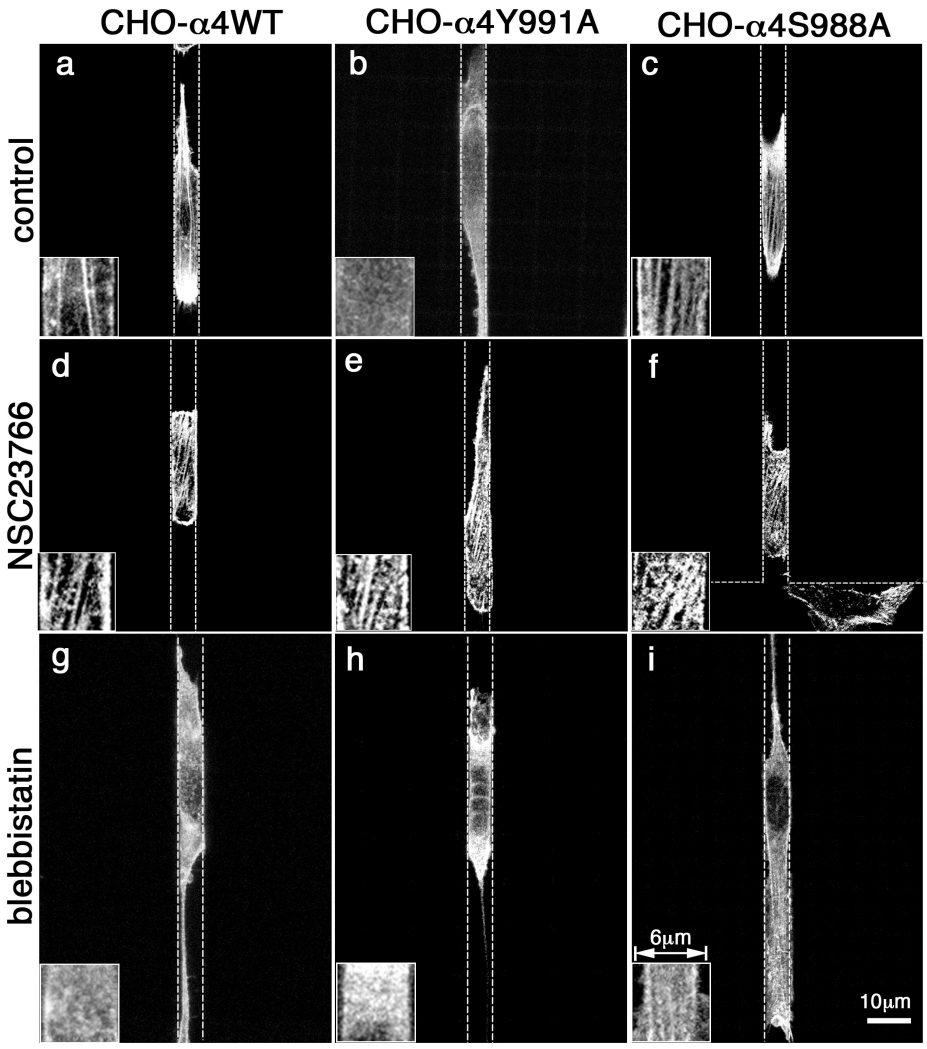

Figure 3-4 Effects of inhibiting Rac1 or myosin II on stress fiber and focal adhesion densities in cells migrating inside 6-μm channels. CHO-α4WT, CHO-α4Y991A, and CHO-α4Y988A cells were induced to migrate inside 6-μm VCAM-1-coated channels in the presence of vehicle control **(*a-c*)**, NSC23766 **(*d-f*)** or blebbistatin **(*g-i*)**. Cells were stained with TRITC-conjugated phalloidin and imaged by confocal microscopy. The box at the lower left corner of each panel shows an enlarged view highlighting the stress fibers. Bar, 10 μm.

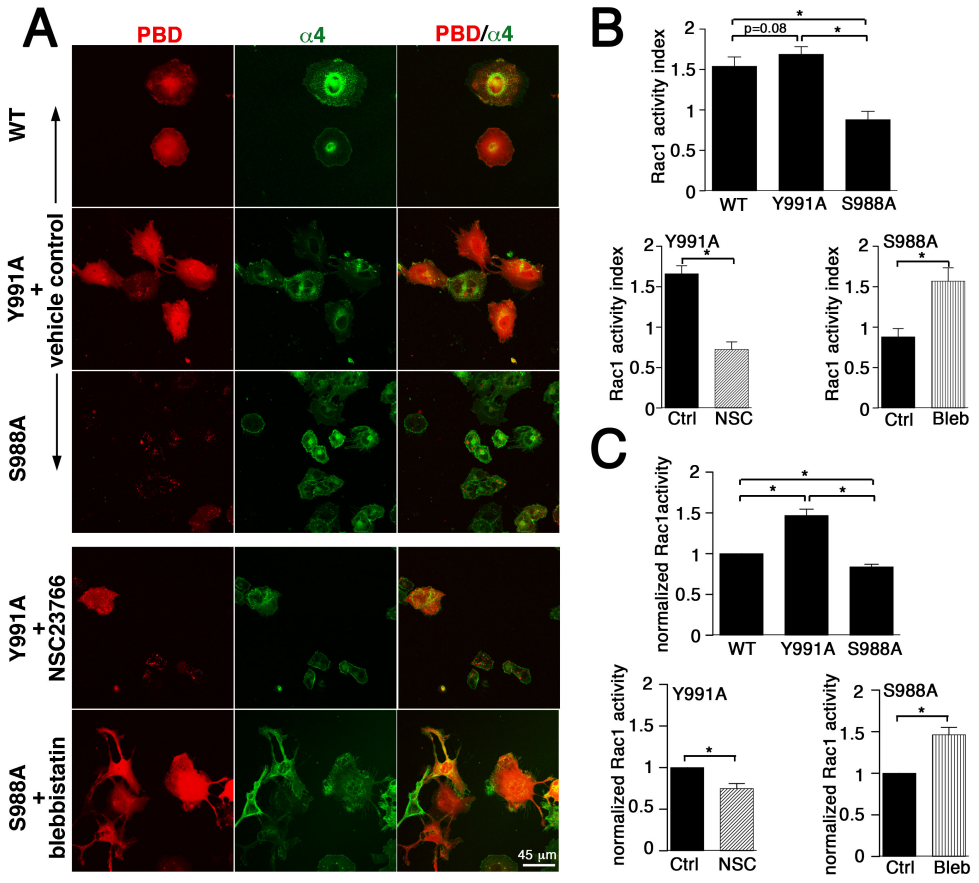

Figure 3-5 Effects of Rac1 or myosin II inhibitors on Rac1 activity. (A) CHO-α4WT, CHO-α4Y991A and CHO-α4S988A cells transfected with RFP-PAK-PBD were plated on VCAM-1 and imaged for GTP-loaded Rac1 (red) and GFP-tagged α4 integrin (green) by dual-color confocal microscopy in presence of vehicle control, NSC23766 for CHO-α4Y991A or blebbistatin for CHO-α4S988A. Bar, 45 μm. **(B)** Rac1 activity was quantified by measuring the RFP-PAK-PBD red fluorescence intensity for each cell type normalized by GFP-tagged α4 integrin. Data represent mean ± SEM of ≥50 cells from 2 independent experiments. **(C)** The overall level of GTP-loaded Rac1 was quantified in presence of vehicle control or indicated treatments using ELISA. Data represent mean ± SEM from 4 independent experiments. *, P <0.05.

3.3.4 α4β1-mediated signaling pathway is required for the migration of invasive melanoma cells

α4β1 integrin is upregulated in human primary invasive melanoma cells (Mostafavi-Pour et al., 2003; Ryu et al., 2007) and plays important roles in melanoma extravasation (Matsuura et al., 1996). Therefore, we tested an invasive melanoma cell line, A375-SM, which expresses high levels of endogenous α4β1 integrin. Like CHO-α4WT, A375-SM cells displayed a fibroblast-like morphology on VCAM-1- or fibronectin-coated surfaces. Moreover, A375-SM cells exhibited a similar dependence of migration velocity on VCAM-1 concentration as the α4β1-expressing CHO cells in wide and narrow channels (**Fig. 2-3A, 3-6A**). In VCAM-1- or fibronectin-coated microchannel, NSC23766 treatment suppressed wide (50- and 20-μm) channel migration but enhanced narrow (6- and 3-μm) channel migration (**Fig. 3-6 B, E**). In contrast, blebbistatin inhibited narrow channel migration without altering the migration velocity through wide channels (**Fig. 3-6 B, E**). Of note, blebbistatin-treated A375-SM cells displayed lamellipodia protrusion and trailing tail defects similar to those observed in blebbistatin-treated CHO-α4WT cells. NSC23766 treatment increased the stress fiber density of cells plated on a 2D surface (**Fig. 3-6 C**) and resulted in thicker stress fibers in cells migrating through 6-μm channels (**Fig. 3-6D**). As expected, blebbistatin diminished stress fiber formation (**Fig. 3-6 C, D**). Thus, high stress fiber levels correlate with high cell migration potential in narrow channels, which is consistent with the data on CHO-α4WT cells.

We next tested the pharmacological inhibitor 6B345TTQ, which specifically disrupts α4/paxillin binding (Kummer et al., 2010). Similar to CHO-α4Y991A cells, treatment of A375-SM cells with 6B345TTQ increased migration velocity in wide channels but suppressed it in narrow channels (**Fig. 3-6F**). Notably, these effects were

abolished when A375-SM cells were co-treated with 6B345TTQ and NSC23766 (**Fig. 3-6F**). NSC23766 also reversed the 6B345TTQ-induced suppression of stress fiber formation (**Fig. 3-6D**). These results demonstrate that the signaling pathway involving α4/paxillin binding and the crosstalk between Rac1 and myosin II is required for efficient migration of A375-SM cells in narrow channels.

We also treated A375-SM cells with an anti-α4 integrin blocking antibody. This treatment markedly reduced the migration velocity in both wide and narrow channels (**Fig. 3-7A**). Blebbistatin and NSC23766 rescued the migratory defect induced by the anti-α4 integrin antibody in wide and narrow channels, respectively (**Fig. 3-7A**). Furthermore, blebbistatin and NSC23766 increased the Rac1 activity and stress fibers, respectively, in anti-α4 integrin-treated A375-SM cells (**Fig. 3-7 D, E**). These results disclose the importance of α4β1 integrin in promoting the migration of A375-SM cells in both unconfined and confined spaces. Like CHO-α4WT cells, A375-SM cells optimize their motile activities by routing the α4β1-mediated signaling network to distinct targets in response to different physical microenvironments.

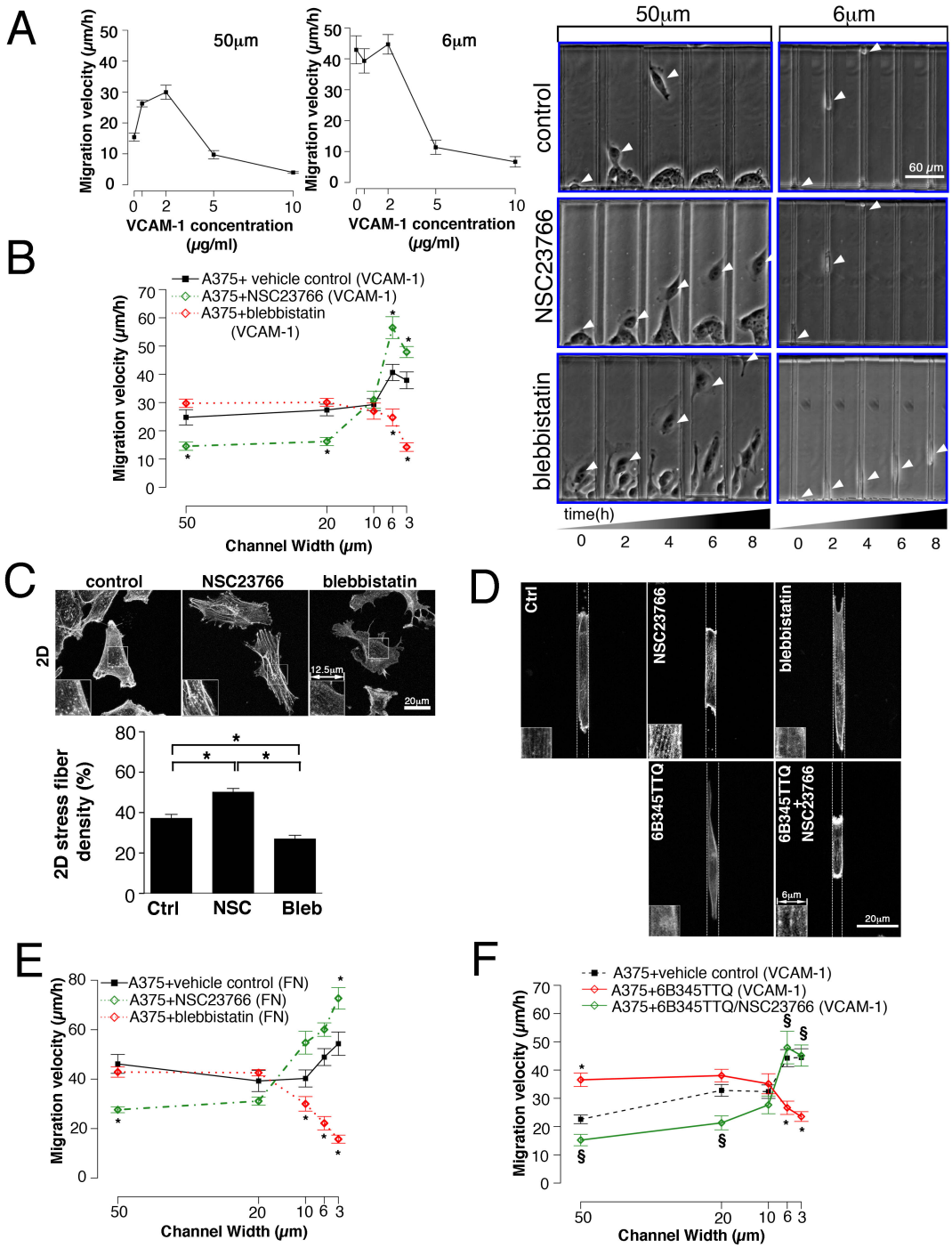

Figure 3-6 Migration of A375-SM cells in microchannels. A375-SM cells were induced to migrate in microchannels coated with VCAM-1 (A-D) or fibronectin (E-F). **(A)** Migration velocity of A375-SM cells as a function of VCAM-1 coating concentration in 50-μm and 6-μm microchannels. (**B** and **E**) A375-SM cells were treated with NSC23766, blebbistatin or vehicle control, and their migration velocities in channels of different widths were quantified. In (**B**), the images of cells migrating

inside the 50-μm or 6-μm channels at designated time-points are shown. White arrowheads, the centroid of cell body. Bar, 60 μm. **(C-D)** A375-SM cells were plated on a 2D surface (C) or induced to migrate inside a 6-μm channel (D) in the presence of vehicle control, NSC23766 or blebbistatin, stained with TRITC-conjugated phalloidin and imaged by confocal microscopy. The box at the lower left corner of each panel shows an enlarged image of stress fibers. Bars, 20 μm. In (C), the density of stress fibers was measured and graphed as percentage of total cell spreading area occupied by stress fibers. Each data (A-E) represent mean ± SEM of >40 cells from 3 independent experiments. *, $P < 0.005$ (B, E) or $P < 0.05$ (C). (**F**) A375-SM cells were treated with the α4/paxillin binding inhibitor, 6B345TTQ, in the presence of NSC23766 or vehicle control. Cell migration velocities in channels of different widths were quantified. Data represent mean ± SEM of >30 cells from 2 independent experiments for each channel width. *, $P < 0.005$ relative to control. §, $P < 0.005$ relative to 6B345TTQ treatment alone.

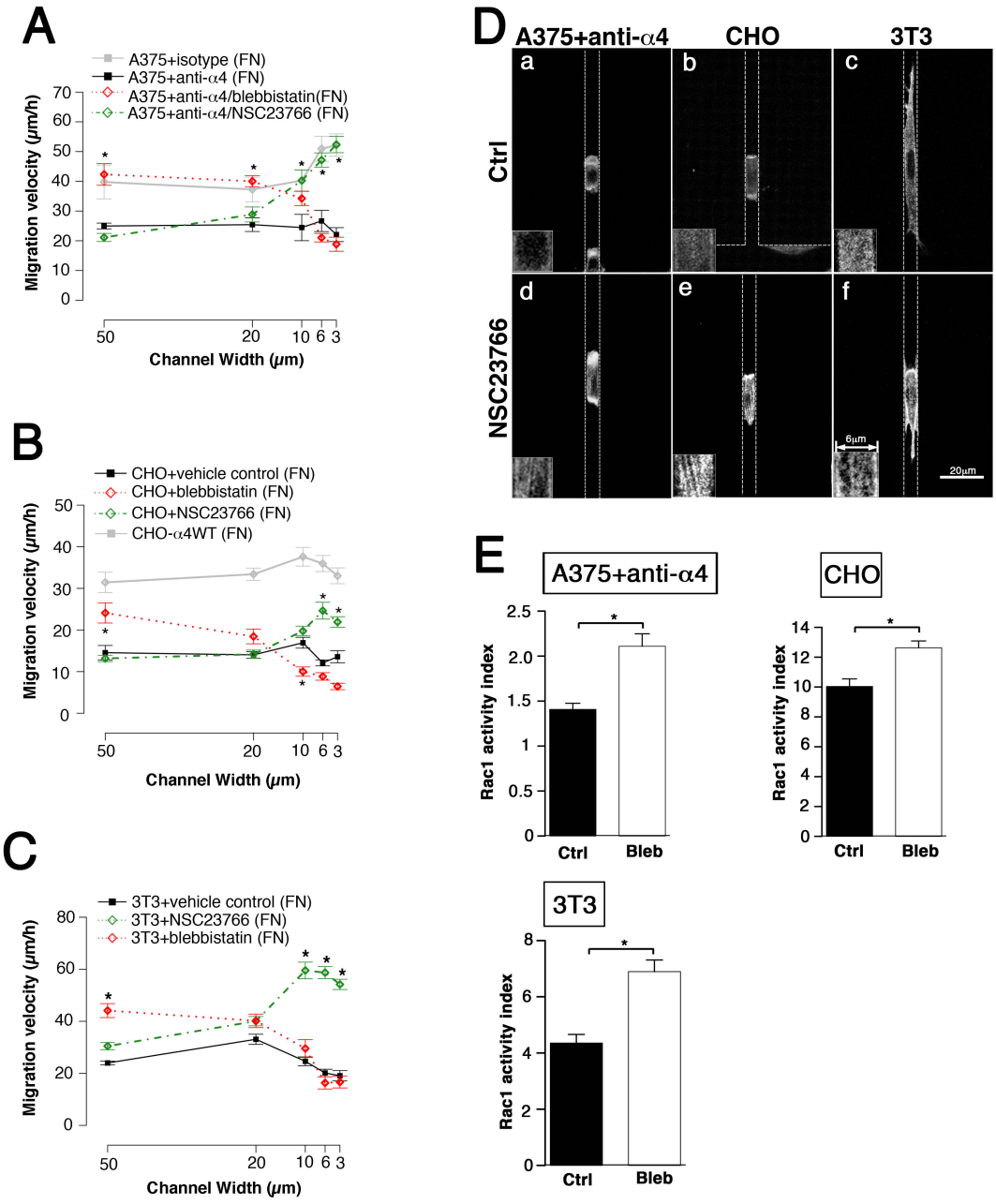

Figure 3-7 Effects of Rac1 and myosin II inhibitors on the migration of A375-SM, CHO cells and 3T3 fibroblasts in microchannels. A375-SM cells treated with an anti-α4 integrin antibody or an isotype control **(A)**, CHO cells **(B)** or 3T3 fibroblasts **(C)** were incubated with with NSC23766, blebbistatin or the vehicle control and allowed to migrate through microchannels coated with fibronectin. Cell migration velocities in channels of different widths were quantified. CHO-α4WT

cells treated with vehicle control were also included for comparison (B). Data represent mean ± SEM of >30 cells from at least 3 independent experiments for each channel width. *, P <0.005 relative to control. (**D**) Cells migrating inside 6 μm channels were stained with TRITC-conjugated phalloidin and imaged by confocal microscopy. The box at the lower left corner of each panel shows an enlarged image of stress fibers. Bars, 20 μm. (**E**) Rac1 activity was quantified by measuring the RFP-PAK-PBD red fluorescence intensity for each cell type normalized by FITC intensity from background using dual-color broad field microscopy. Data represent mean ± SEM of ≥85 cells. *, P <0.05.

3.3.5 The migration of CHO cell and 3T3 fibroblast in wide and narrow channels is attenuated by myosin II and Rac1, respectively

The results from the anti-α4 integrin antibody experiments (**Fig. 3-7 A, D, E**) suggest that the rescue by NSC23766 and blebbistatin in the microchannels could be a general phenomenon for fibroblast-like cells that are devoid of α4β1 integrin. To test this, we assessed the migratory potential of parental CHO cells and 3T3 fibroblasts in the microchannel assay in the presence and absence of NSC23766 or blebbistatin. In line with anti-α4 integrin-treated A375-SM cells, the parental CHO cells displayed a reduced migration velocity compared to CHO-α4WT cells in fibronectin-coated wide and narrow channels; Blebbistatin and NSC23766 increased CHO cell migration velocity in wide and narrow channels, respectively **(Fig. 3-7B)**. Moreover, blebbistatin and NSC23766 increased Rac1 activity and stress fiber density of CHO cells, respectively (**Fig. 3-7D, E**). Similar observations were made with 3T3 fibroblasts (**Fig. 3-7 C, D, E**). These data demonstrate that, in fibroblasts, myosin II and Rac1 can function as breaks through a crosstalk mechanism to attenuate the migration of the cells on unconfined and confined microenvironments, respectively.

CHAPTER 4

Myosin II A and Myosin II B differentially regulate confined and unconfined migration

4.1 Introduction

The myosin superfamily of actin-based molecular motors consists of at least 25 different classes. The myosin II subfamily, which includes skeletal, cardiac and smooth muscle myosins, as well as nonmuscle myosin II (NMII), has the most members. In vertebrates, there are over 15 different myosin II isoforms, each of which contains a different myosin II heavy chain (MHC). This MHC diversity is generated by multiple genes as well as by alternative splicing of the pre-mRNA that encodes them.

Myosin II molecules are hexamers composed of MHC dimers and two pairs of myosin light chains (MLCs), and can bind reversibly to actin filaments, hydrolyze ATP in a process that is activated by actin and thereby convert chemical energy into mechanical force and movement. Although this contractile activity is most evident in differentiated muscle tissues, such as the beating heart, it is also seen in nonmuscle cells in diverse cellular processes such as cell division, cell migration, and cell-cell and cell-matrix adhesion. There is, however, a fundamental difference in regulation within the vertebrate myosin II subclass. Whereas the primary regulation of skeletal and cardiac muscle myosin II is through a set of actin-associated proteins – troponin and tropomyosin – the regulation of vertebrate nonmuscle and smooth muscle myosin II is through phosphorylation of the 20 kDa MLC(Vicente-Manzanares et al., 2009).

This latter type of regulation permits nonmuscle and developing muscle cells to respond to numerous signals originating both outside and inside the cell.

Whereas the N-terminal globular head of the molecule contains the MgATPase catalytic domain, the α-helical coiled-coil Cterminal domain is involved in filament formation. Thus, myosin can be viewed as a bipartite molecule that has two distinct but related functions. One is manifested by its ability to translocate actin filaments and resides in its globular motor domain and lever arm. This ability to act as a motor permits a number of different roles. For example, myosin plays a role in cell migration both by moving the body of the cell forward and by retracting the rear of the cell, and it can redistribute inside cells, thus playing a role in generating cell polarity. The second function of NMII is structural and resides in the ability of the rod portion of the molecule to form filaments, which allows several myosin heads to maintain tension for long periods of time, similarly to smooth muscle myosin. Both functions require binding to actin. The recent availability of mutant forms of NMII with compromised motor activity has permitted separation of these functions in both cultured cells and mice.

In general, NMII provides contractility in cell migration and this process is facilitated by phosphorylation of myosin light chain (MLC). It has reported that several kinases catalyze this phosphorylation. Myosin light chain kinase and Calcium interaction together activate MLCK, which in turn promotes phosphorylation of MLC. However, Rho kinase can phosphorylate MLC via activating MLCK itself or by inhibiting the subunit of myosin phosphatase (Wilkinson et al., 2005). Moreover, some researches have shown that MLCK and Rho kinase activate MLC in spatial regulation. MLCK regulates MLC in cell periphery and in contrast Rho kinase is more active in cell center, where focal adhesion formation is regulated(Totsukawa et

al., 2000). Moreover, Rho kinase preferentially regulates the phosphorylation of MIIA myosin light chian in cell center, which implies that difference kinase(Totsukawa et al., 2000) might have differential regulation of myosin II iso-forms (Sandquist et al., 2006). Accumulated evidence show that MIIA and MIIB function differentially during cell migration (Even-Ram et al., 2007; Kolega, 2006; Vicente-Manzanares et al., 2007). More researches have indicated that the primary role of MIIA is to provide contractile force, but not exclusively, MIIB is more responsible of generating the force of lamellipodia ruffle in cell leading edge (Giannone et al., 2007).

Because of the critical roles of myosin II in cell migration, in this chapter, using our microchannel assay, we sought to investigate the differential roles of MIIA and MIIB in response to different degree of physical confinement.

4.2 Materials & Methods

4.2.1 Myosin II A and Myosin II B plasmid and transfection

The pSUPER-MIIA, pSUPER-MIIB, siRNA-insensitive MIIA and MIIB were gifts from Alan F. Horwitz (University of Virginia, Chalottesville, VA). In pSUPER-MIIA and pSUPER-MIIB, the oligonucleotides G A T C T G A A C T C CT T C G A G C (IIA) and G G A T C G C T A C T A T T C A G G A (IIB) were inserted into the appropriate pSUPER cassette. In siRNA-insensitive MIIA and MIIB plasmids, MIIA and MIIB cDNA, each carrying a silent mutation, were inserted into an mCherry vector modified from pEGFP-C1 (Vicente-Manzanares et al., 2007). The RFP-PAK-PDB (in a modified pUW vector) was a gift from Peter Devreotes (JHU, Baltimore, MD). Transient transfection was performed using Lipofectamine 2000 (Life Technologies) according to the manufacturer's protocol. Knockdown efficiency was verified by Western blotting analysis using antibodies against MIIA (Sigma), MIIB (Santa Cruz Biotechnology) and β-actin (Sigma).

4.3 Results & Discussion

4.3 MIIA and MIIB have distinct roles in wide versus narrow channel migration

The differential effects of blebbistatin on wide versus narrow channel migration prompted us to examine the relative contributions of non-muscle myosin II isoforms to cell migration through these microchannels. The major non-muscle myosin II isoforms, IIA (MIIA) and IIB (MIIB), share the basic ATPase-dependent motor functions of binding and contracting F-actin, but they have distinct enzymatic kinetics (Kelley et al., 1996), subcellular distributions (Cai et al., 2006; Kelley et al., 1996) and functions (Stroka and Aranda-Espinoza, 2011). We knocked down each isoform in CHO-α4WT cells by transiently expressing MIIA- or MIIB-siRNA in the cells. The efficacy of MIIA or MIIB depletion was verified by immunoblotting (**Fig. 4-1A**). MIIA-depleted CHO-α4WT cells exhibited increased lamellipodia protrusion and a trailing tail phenotype (**Fig. 4-1B**) similar to that displayed by MIIA-depleted fibroblasts (Doyle et al., 2009; Even-Ram et al., 2007) and blebbistatin- and Y27632-treated CHO-α4WT cells (**Fig. 2-3**). Like the blebbistatin and Y27632 treatments, MIIA depletion in CHO-α4WT cells failed to alter wide (50- and 20-μm) channel migration but markedly suppressed narrow (6- and 3-μm) channel migration (**Figs. 4-1B and 4-2**). In distinct contrast, MIIB-depleted CHO-α4WT cells exhibited poor spreading (**Figs. 4-1 and 4-2**), resulting in a dramatic reduction of wide channel migration (**Fig. 4-1B**), whereas the inhibitory effect became less pronounced as the channel width decreased ($P>0.06$ at 6- and 3-μm channels). Furthermore, the inhibitory effects of MIIA- or MIIB-siRNA were rescued by co-transfection of siRNA-insensitive MIIA or MIIB, respectively **(Fig. 4-2)**. Thus, while depleting MIIA had similar effects as blebbistatin and Y23766, depleting MIIB displayed similar effects as the Rac1 inhibitor NSC27632.

Both MIIA and MIIB are activated by myosin light chain kinase (MLCK). We therefore tested the effect of blocking MLCK by treating cells with a specific MLCK inhibitor, ML-7 (25 μM). This intervention suppressed cell spreading and inhibited CHO-α4WT cell migration in both wide and narrow channels (**Fig. 4-1C**).

Collectively, our data reveal that MIIA and MIIB have distinct roles in wide versus narrow channel migration. MIIA is required for narrow channel migration and MIIB for wide channel migration, whereas MLCK is required for both wide and narrow channel migration.

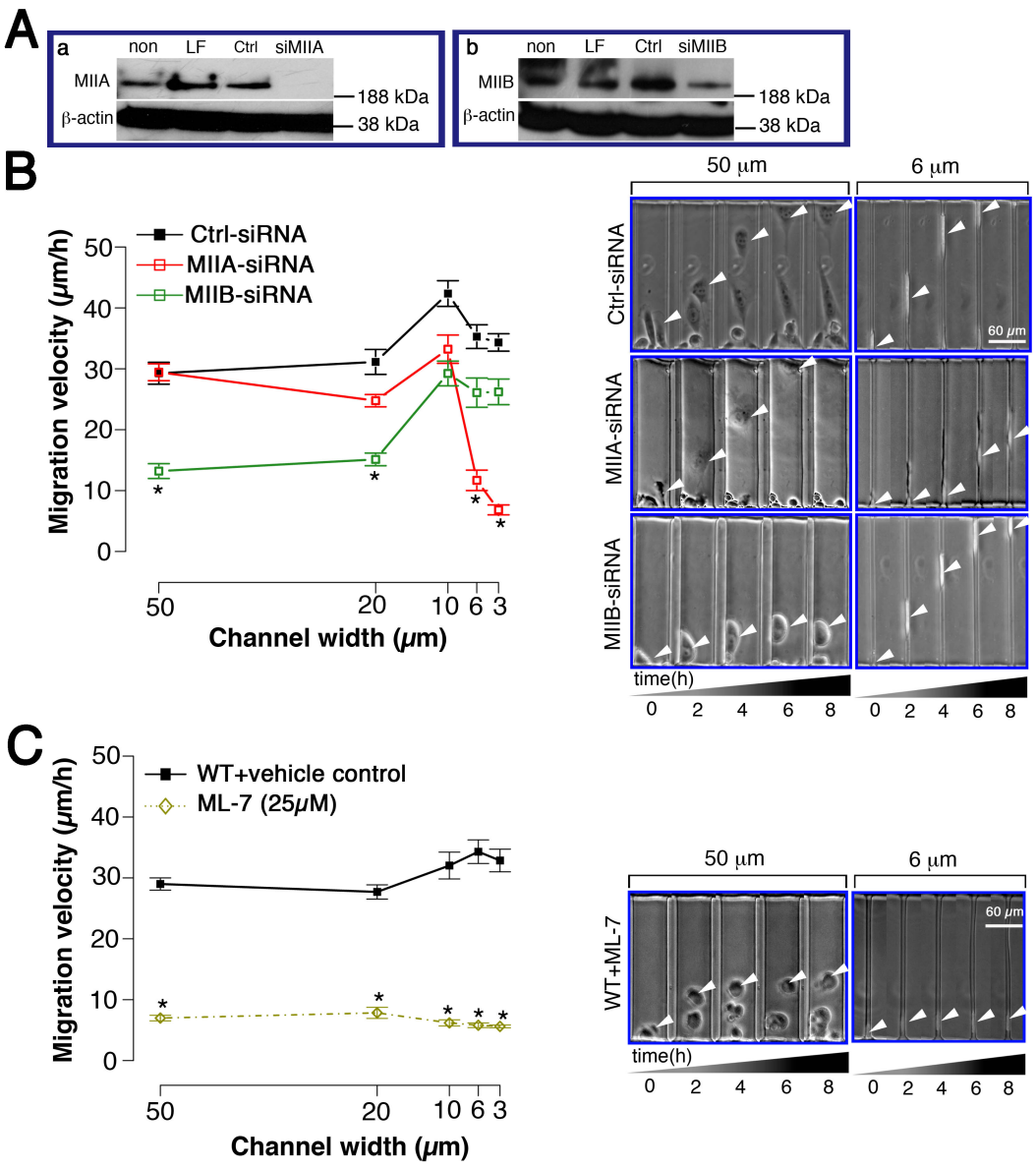

Figure 4-1 Effects of MIIA- or MIIB-depletion on the migration of CHO-α4WT cells in microchannels. (A) CHO-α4WT cells were either transfected with an siRNA for MIIA ***(a)*** or MIIB ***(b)*** or a control siRNA (Ctrl), or with lipofectamine only (LF) or remained untransfected (non). The depletion of either MIIA or MIIB by their corresponding siRNAs was demonstrated by immunoblotting using an anti-MIIA or anti-MIIB antibody. β-actin served as an internal control. **(B)** The migration velocities of MIIA-, MIIB-depleted CHO-α4WT cells and siRNA controls were quantified as a function of channel width. **(C)** The migration velocity of CHO-α4WT cells, treated

with either ML-7 or a vehicle control, was measured in channels of different widths. In (B) and (C), all channels were coated with VCAM-1. Data represent mean ± SEM of >45 cells from 3 independent experiments. *, P <0.005. The images of cells migrating inside 50-μm or 6-μm microchannels at designated time-points are also shown. White arrowheads, the centroid of cell body. Bar, 60 μm.

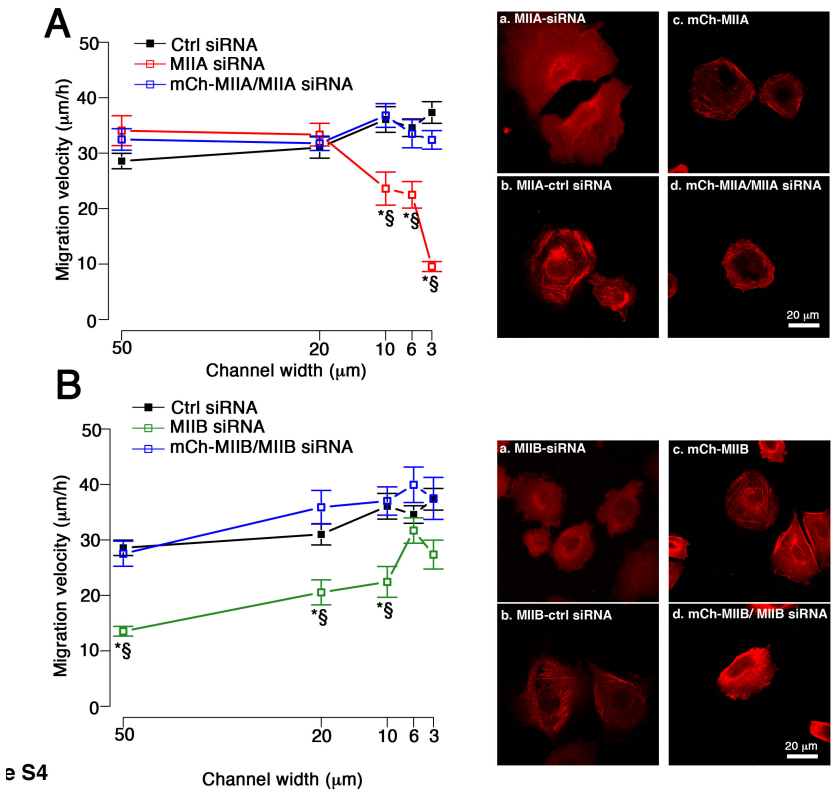

e S4

Figure 4-2 Rescue of migration defect of MIIA- or MIIB-depletion by cotransfection with mChe-MIIA or mChe-MIIB in CHO-α4WT cells. Cells were transfected with either MIIA siRNA (60 nM) or scramble control or co-transfected with MIIA siRNA and mCherry-MIIA (1 ng/ml) (60 nM) **(A)**. Similarly, cells were transfected with MIIB siRNA (60 nM) or scramble control or co-transfected with MIIA siRNA and mCherry-MIIB (1 ng/ml) (60nM) **(B)**. The depletion and rescue of MIIA and MIIB were confirmed by the absence or presence of stress fibers visualized by immunofluorescent staining with antibodies against MIIA (Aa and b) or MIIB (Ba and b), or by the fluorescence of mCherry (Ac and d for MIIA; Bc and d for MIIB). The migration velocity of MIIA-, MIIB-depleted, and MIIA, MIIB-rescued or scramble control CHO-α4WT cells inside microchannels of different widths was quantified. Data represent mean ± SEM of >25 cells from ≥2 independent

experiments. *, P < 0.005 relative to a control siRNA. §, P< 0.005 relative to mCherry-MIIA/siRNA-MIIA or mCherry-MIIB/siRNA-MIIB.

CHAPTER 5

Confined migration of α4β1 expressing T-cells is regulated by Rac1/myosin II pathway

5.1 Introduction

Leukocytes are highly migratory cells that can develop a spectrum of versatile migration strategies to enter and transmigrate through various tissues and organs(Friedl and Brocker, 2000; Hauzenberger et al., 1995; Springer, 1994). In the body, migrating leukocytes adapt their cell bodies to preexisting structures, yet appear simultaneously able to structurally modify matrix barriers. Putatively nondestructive T cell migration occurs within the loose connective tissue of lymphatic organs and interstitial compartments(Hauzenberger et al., 1995). These compartments comprise the lymph node cortex, the mesentery, perivascular fibrillar trails along blood vessels, or the dermal papillae(Friedl et al., 1998; Hauzenberger et al., 1995). It has been well studied that to reach inflammatory side, T lymphocytes perform crawling along the surface of other cells, such as vessel endothelium before transmigration, fibroblastic reticulum cells in lymph nodes (Gretz et al., 1997), and antigen-presenting cells(Gunzer et al., 2000). For both cancer cells and T lymphocytes, the infiltration of basement membranes requires attachment integrated with proteolytic mechanisms(Leppert et al., 1995) and profound shape changes. In chronic inflammation, the interaction of T cells with resident tissue cells can result in severe proteolytic remodeling of tissue architecture, integrity, and function(Mach et al., 1999). For all of these conditions, migratory traction occurs in conjunction with

recognition of additional activation signals from the counterpart cell or matrix interphase, implicating overlapping pathways of cytoskeletal dynamics and signal transduction. Such a broad spectrum of migratory capabilities through or across biophysically and biochemically very different substrates implies a great degree of flexibility and adaptability of leukocyte migration and positioning strategies. Such diversity may set leukocytes apart from other more specialized migratory cell types. As examples, fibroblasts, keratinocytes, and neurons migrate only under circumstances highly restricted in location and time, i.e., on morphogenesis or wound healing within a specific tissue context.

Cell migration within the tissues is a complex mechanochemical process that requires the integration of key events in signaling, cytoskeletal, membrane, and adhesion systems. Based on cell type-specific morphological and functional criteria of migration within an extracellular matrix (ECM) environment, i.e., polarization and shape change, migration velocity, cytoskeletal organization, and integrin and protease expression and function, at least three migratory prototypes can be classified: (1) amoeboid crawling can be distinguished from (2) fibroblast-like, mesenchymal migration and collective cell movement, as seen in multicellular strands, sheets, or clusters.

The concept of amoeboid movement is most clearly established by studies using the single-cell stage of the lower eukaryotic ameba Dictyostelium discoideum(Mach et al., 1999). Amoeboid movement results from alternating cycles of morphological expansion and contraction driven by cytoskeletal dynamics, shape change where less stress fiber formation/focal adhesion is required. Amoeboid migration allows to rapidly adapt especially 3D environment in order to develop high migration velocities transmigrating physiological barriers. Moreover this featured movement has been

observed in higher eukaryotes, most notably for neutrophils, lymphocytes, and some tumor cells(Springer, 1994; Stossel, 1994).

α4β1 integrin are important adhesion/migration molecules of T-cells that confer mechanical stability on interactions between cells and their environment. The well-known function of α4β1 of T-cells is its adhesive function to vascular-cell adhesion molecule 1 (VCAM-1) and mucosal addessin-cell adhesion molecule 1 (MAdCAM-1). It has been well established that molecular interaction is critical for T-cells to traffic in central nervous system and intestine. In contrast, the accumulated evidence shows that in CNS micro-vessel where the diameter is limited to several microns and fluid speed is reduced, T-cell employs α4β1 signaling to trigger amoeboid migration to fast move along those micro-vessel (von Andrian and Engelhardt, 2003).

In this chapter, inheriting the concept of featured confined migration mode in fibroblast-like cells, using microchannel assay, we sought to reveal the α4β1-mediated mechanistic switch between amoeboid and fibroblast-like, mesenchymal migration in Jurkat T-cell and $CD4^+$ T cells isolated from mice.

5.2 Materials & Methods

5.2.1 Jurkat T-cell culture

Jurkat T cells and primary $CD4^+$ cells were treated with 20 μM NSC23766, 75 μM blebbistatin, 90 μM 6B345TTQ or appropriate vehicle controls. For antibody blocking experiments, cells were treated with 3 μg/ml of anti-α4 integrin mAb (clone P1H4, Millipore). After 1 h of incubation with the inhibitors or antibody at 37 ^oC, the chemoattractant (10% FBS) was added to topmost inlet port

5.2.2 T-cell isolation

Mice were kept in accordance with guidelines of the Johns Hopkins University Institutional Animal Care and Use Committee. α4Y991A mice carrying a targeted α4Y991A mutation, backcrossed into a C57BL/6 background, were a gift from Mark H. Ginsberg (Feral et al., 2006). Wild-type C57BL/6 mice were obtained from Jackson Laboratories. The mice were sacrificed via CO_2 asphyxiation. Spleens and lymph nodes were collected and homogenized, and red blood cells were lysed. $CD4^+$ T cells were purified using Miltenyi magnetically labeled beads (Miltenyi Biotec) according to the manufacturer's protocol. Cells were then cultured in 50% RPMI/50% EHAA media supplemented with 10% heat-inactivated low-LPS FBS, 1% penicillin/streptomycin, and 1% glutamine and stimulated with plate-bound anti-CD3 (145-2C11) in combination with anti-CD28 (2 μg/ml) antibodies for 72 h (**Fig 5-1**).

5.3 Results & Discussion

The migration of T lymphocyte is promoted by α4/paxillin binding and the downstream Rac1-myosin II crosstalk pathway

α4β1-integrin is highly expressed in T lymphocytes (Yednock et al., 1992). T lymphocytes display an amoeboidal mode of migration, which is distinct from that of fibroblast-like cells such as α4β1 integrin-expressing CHO and A375-SM melanoma cells. We thus sought to investigate the migratory phenotype of the Jurkat T cell line and primary T cells. Reminiscent to CHO-α4WT and A375-SM cells migrating in narrow channels, the migration velocity of Jurkat T cells was suppressed by blebbistatin but was enhanced by NSC23766, albeit in all channels (**Fig. 5-2A**). The migratory potential of T cells on 2D is negatively correlated with their spreading area (Jacobelli et al., 2010). Thus, we also measured this parameter. Blebbistatin and NSC23766 increased and reduced, respectively, the spreading area of Jurkat T cells on VCAM-1-coated 2D surfaces **(Fig. 5-2D)**. To determine if α4/paxillin binding contributes to Jurkat T cell migration, cells were treated with 6B345TTQ (22.5 μM),

which specifically disrupts α4/paxillin binding. 6B345TTQ significantly reduced the migration of Jurkat T cells in all channels and increased their spreading area **(Fig. 5-2B, E)**, which is in line with published data on 2D (Kummer et al., 2010). Furthermore, co-treatment with 6B345TTQ and NSC23766 abolished the effect of 6B345TTQ on the migration velocity and cell spreading (**Fig. 5-2B, E**).

We also tested primary $CD4^+$ T cells isolated from mice carrying the α4Y991A mutation generated by gene targeting (Feral et al., 2006) (referred as to α4Y991A-$CD4^+$), and those from wild-type mice (referred as to WT-$CD4^+$). α4Y991A-$CD4^+$ cells exhibited larger spreading area when plated on 2D surface and reduced migration velocities relative to WT-$CD4^+$ in all channels (**Fig. 5-2C, F**), which is in concert with the reported spreading and 2D migration phenotypes of Jurkat T cells carrying the α4Y991A mutation (Liu et al., 1999). Notably, the migration and spreading defects of α4Y991A-$CD4^+$ cells were rescued by NSC23766 (**Fig. 5-2C, F**). We thus conclude that α4/paxillin binding and its inhibitory effect on Rac1 promotes effective migration of T cells via Rac1-myosin II crosstalk, which is analogous to the migration of CHO-α4WT and A375-SM cells in narrow channels.

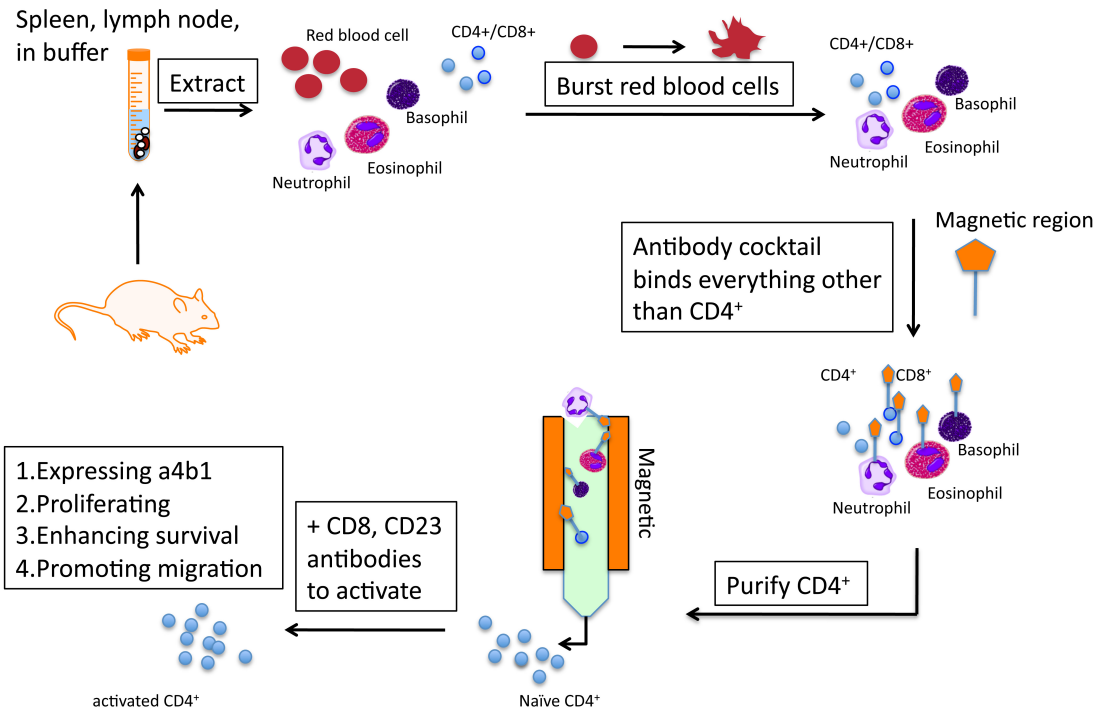

Figure 5-1 Procedures of isolating T-cell

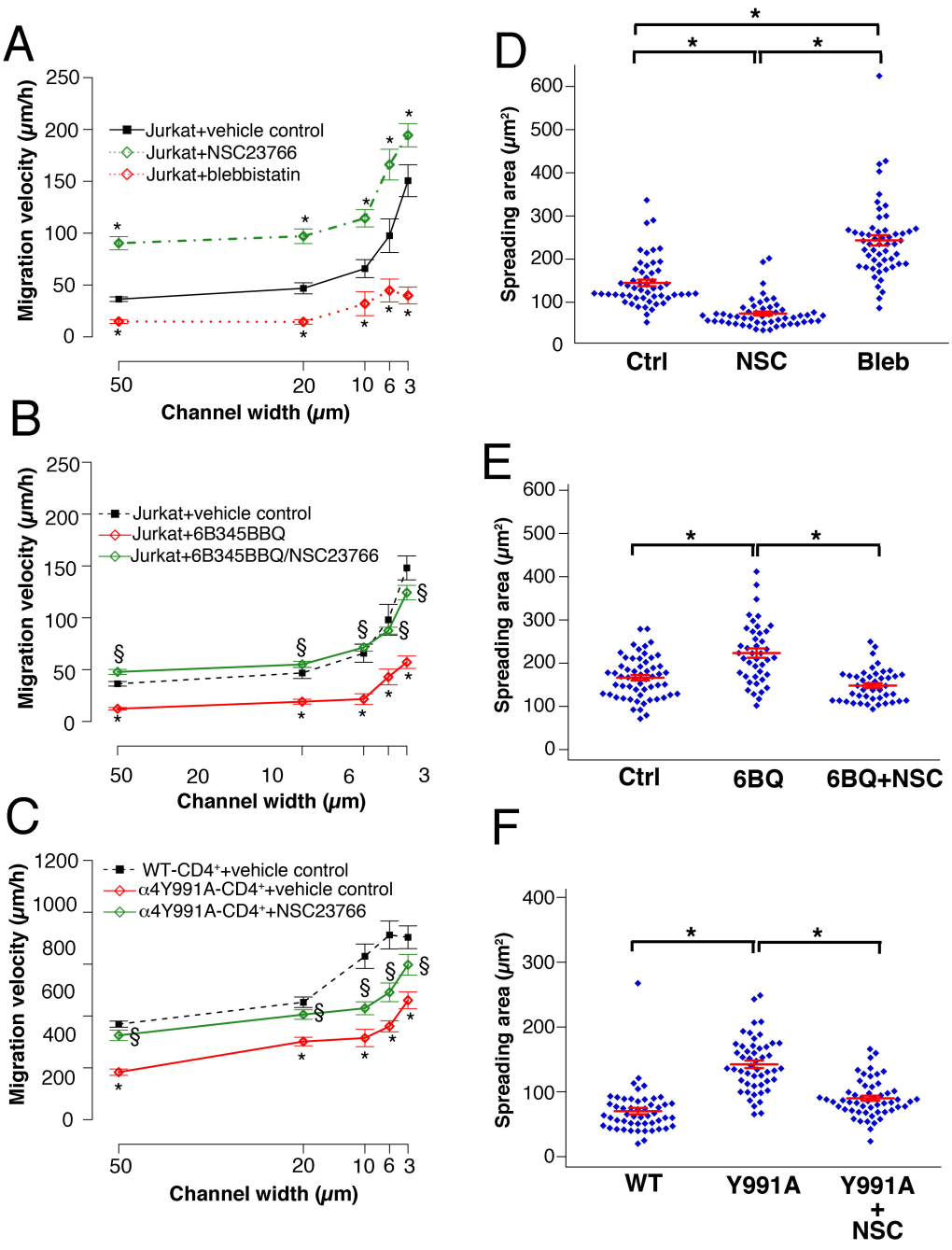

Figure 5-2 Effects of Rac 1 and myosin II inhibitors on the migration of Jurkat T and primary CD4$^+$ T cells in microchannels. (A, D) Jurkat T cells were treated with NSC23766 (NSC) or blebbistatin (Bleb) or vehicle control (Ctrl). (**B, E**) Jurkat T cells were treated with the α4/paxillin binding inhibitor, 6B345TTQ, or vehicle control, or 6B345TTQ plus NSC23766 or vehicle control. (**C, F**) Primary WT-CD4$^+$ or Y991A-CD4$^+$ T cells were treated with vehicle control or NSC23766. Cells were either

induced to migrate through channels of different widths (A-C) or plated on a 2D surface (D-E). All surfaces were coated with VCAM-1. Cell migration velocities (A-C) and mean spreading areas (D-E) were quantified. Data represent mean ± SEM of >60 cells. *, $P < 0.005$ relative to control (A, B) or WT-$CD4^+$ T cells (C). §, $P < 0.005$ compared to the absence of NSC23766.

CHAPTER 6

Cell modulates protein kinase A activity to optimize confined/unconfined migration

6.1 Introduction

Cell migration in response to growth factors and chemoattractants is essential for embryonic development, tissue homeostasis, and the immune response(Knight et al., 2000). It is also a major factor in the pathogenesis of many human diseases, including cancer(Stetler-Stevenson et al., 1993). This complex process involves dynamic and coordinated interactions among integrins, chemoattractant receptors, and the actin cytoskeleton, which result in actin polymerization at the leading edge and contraction of actin bundles within the cell body to promote translocation. These dynamic changes in the actin cytoskeleton are initiated by the engagement of chemoattractant and integrin receptors on the cell surface with the respective ligands. Such interactions trigger cascades of outside-in signaling that results in the remodeling of the actin cytoskeleton and consequent directed movement(Liu et al., 1999; Moyano et al., 2003; Nishiwaki et al., 2000; Urbano et al., 2011). To understand the mechanism of cell migration in different physical environemnt, these signaling events need to be defined and linked to cell surface receptors, actin dynamics, and local geometry. Members of the Rho family of GTPases, including Rho/myosin II pathway, Rac1, Cdc42, Arp2/3 complex, and Wiskott-Aldrish syndrome protein (WAVEs) are considered to be key signaling intermediates for cell migration as discussed in previous chapters.

Recent studies have highlighted an important role for cAMP/PKA metabolism in the migration of carcinoma cells and in the regulation of RhoA and Rac1 function in several cooperative pathways (Backert et al., 2010; Brandt et al., 2009; Newell-Litwa and Horwitz, 2011; Zimmerman et al., 2012). For example, α4 integrin expressing in wide variety of cell line such as fibroblast-like melanoma and leukocytes plays very important role of enhancing the cell migration in different degree of confinement and various physical constraint. It has reported that the phosphorylation of the α4 cytoplasmic domain by c-AMP–dependent protein kinase A (PKA) inhibits paxillin binding and is restricted to the leading edge of broad protrusive lamellipodia(Liu et al., 1999; Nishiya et al., 2005). This localized phosphorylation of α4 at the leading edge is critical for optimize α4β1-mediated 2D migration(Goldfinger et al., 2003). However, we have found that when cell encounters physical constraint, α4β1 integrin could optimize confinement migration by up-regulating RhoA/myosin II pathway. However, the how confined cells receive the signal from upstream sensor to regulate this process still remains unknown.

The spatiotemporal PKA activity plays an important role of variety of cellular processes, such as survival, proliferation, and migration. PKA phosphorylates numerous protein substrates such as ion channels, GTPases, and transcription factors. The substrate specificity of PKA in vivo is controlled by its subcellular compartmentalization and is mediated by interactions of its regulatory subunits with A-kinase anchoring proteins (AKAPs). For example, Arp2/3 stimulating actin branching is recruited by an AKAP, WAVE, which also provides an anchor site for PKA to associate, thus enriching cell protrusion in several cell types. Moreover, α4 cytoplasmic tail also serves as an AKAP and α4 phosphorylation results in Rac1

activation. Therefore, the interplay of local activated PKA, α4 phosphoryaltion, and AKAPs accessibility in response to physical constraint together determines the migration efficiency.

In this Chapter, we have developed Förster resonance energy transfer (FRET)-based PKA kinase activity reporters that permit the real-time measurement of bulk PKA activity in the cytoplasm of a living cell. Here, we specifically examine the localization of PKA activity at the plasma membrane of living cells using a membrane-targeted reporter, AKAR4-Kras. We showed that cell locally and integratedly modulates its membrane-PKA activity in response to different physical constraint.

6.2 Materials & Methods

6.2.1 cell culture and treatments

CHO-α4WT were generated by stably transfecting CHO cells with pQN4G plasmids, in which wild-type or mutant α4 integrin cDNA was inserted into a PGBI25-fN1 GFP vector (Dikeman et al., 2008; Pinco et al., 2002). The cells were maintained in Ham's F12 (Cellgro, 10-080-CM, company) medium. CHO cells were maintained in DMEM (high glucose, Life technology). Media were supplemented with 10% fetal bovine serum (FBS, Gibco) and 1 μg/ml penicillin/streptomycin. For inhibitor studies, 50 μM forskolin (Santa Cruz), 50 μM Rp-cAMPs (Santa Cruz), or appropriate vehicle controls were added to the cells seeded in serum-free medium near microchannel entrances. Transient transfection was performed using Lipofectamine 2000 (Life Technologies) according to the manufacturer's protocol.

6.2.2 PKA biosensor transfection and imaging

Cells were washed twice with Hanks' balanced salt solution buffer and maintained in the dark at room temperature. Cells were imaged on a Zeiss Axiovert 200M microscope with a cooled charge-coupled device camera (MicroMAX BFT512, Roper Scientific, Trenton, NJ) controlled by METAFLUOR 6.2 software (Universal Imaging, Downingtown, PA). Dual cyan/yellow emission ratio imaging used a 420DF20 excitation filter, a 450DRLP dichroic mirror, and two emission filters [475DF40 for CFP and 535DF25 for YFP]. These filters were alternated by a filter-changer Lambda 10–2(Sutter Instruments, Novato, CA). Exposure time was 50–500 ms, and images were taken every 10–30 s. Fluorescence images were background-corrected by subtracting the fluorescence intensity of background with no cells from the emission intensities of cells expressing fluorescent reporters. The ratios of yellow/cyan emissions were then calculated at different time points. The values of all time courses were normalized by dividing each by the average basal value before drug addition.

6.2.3 1D patterning

A custom mask with 8μm wide linear line was generated using Adobe Illustrator (Adobe), printed on a transparency at high resolution (Pageworks) and used to generate master mold. The general procedure using silicon mold to make PDMS stamp is similar to the protocol of PDMS micro-fluidic in Chapter 2, Materials and Methods. Stamps were then cut out and sonicated in ethanol before each use. Stamps were dried under a nitrogen stream and then coated with a 50mg/ml solution of fibronectin for 30 minutes. To check patterning, stamps were occasionally coated with a mixture of 50 mg/ml fibronectin, rabbit polyclonal anti-fibronectin antibody

(Calbiochem, Gibbstown, NJ) at 1:10 dilution, and Alexa Fluor 488 goat anti-rabbit secondary antibody at 1:100 dilution. Before stamping, 35-mm glass bottom dishes were cleaned with ethanol and oxygen plasma. Dishes were stamped with fibronectin for 1 minute, heated to 140℃ for 30 seconds (Fink et al., 2007), and passivated with 0.1 mg/ml PLL(20)-g-[3,5]-PEG(2) (Susos AG, Dubendorf, Switzerland) in 10 mM HEPES (pH 7.4) for 30 minutes to render the unstamped regions of the dish resistant to cell adhesion (Thery and Piel, 2009). Plates were then washed in PBS and stored at 4℃ for up to 2 weeks or immediately used for cell seeding. Stamps were cleaned with Scotch tape (3M, St Paul, MN) after use.

6.3 Results & Discussion

6.3.1 CHO-α4WT cells reduced α4 phosphorylation level in confined migration

The finding that both CHO-α4WT cells and CHO-α4S988A migrating through narrow channels (6-μm and 3-μm in width) displayed optimal motility suggests that α4 phosphotylation level is reduced to optimize confined migration. To investigate the phosphorylation level of α4 in response to physical confinement, we applied novel microchannel assay. In this assay, cells were first seed in the 2D seeding area and then allowed to migrate toward chemoattractant source through fibronectin-coated channels of fixed height (10μm) and length (200μm) but variable widths (20μm, 10μm, 6μm, and 3μm) (Fig. 6-1A). Migrating cells expressing GFP-tagged α4 were fixed and stained with antibody against phosphorylated α4 integrin and imaged by confocal microcopy. Unconfined CHO-α4WT cells demonstrate highest α4 phosphorylation level, however the α4 phosphorylation level was gradually reduced as degree of confinement increases (Fig. 6-1B). Cells migrating in narrow channels (6μm and 3μm in width) display bipolar α4 phosphorylation pattern and the

α4 phosphorylation level was significantly reduced relative to CHO-WTα4 cells on 2D surface (Fig. 6-1B and C).

It has reported that cells utilize myosin II A to achieve efficient 1D migration (Doyle et al., 2009) and this mechanism is analogous to confined migration in our previous study (Hung et al., 2013). Because α4 phosphorylation regulates myosin II pathway via attenuating Rac1 activity, we also examined the α4 phosphorylation level in response to this confinement engineered by microp-patterning. We generated 8μm-wide fibronectin-printed line where cells were allowed to adhere to form an elongated shape (Fig. 6-1D). Similar phenomena were also observed between cells on 1D pattern and confinement. Using CHO-α4S988A cells as negative control, CHO-α4WT cells on 1D fibronectin pattern displayed significantly lower α4 phosphorylation level relative to ones on 2D printed surface (Fig. 6-1D and E). These data revealed that both physical and adhesive confinement down-regulates α4-phosphorylation in α4β1-integrin expressing CHO cells.

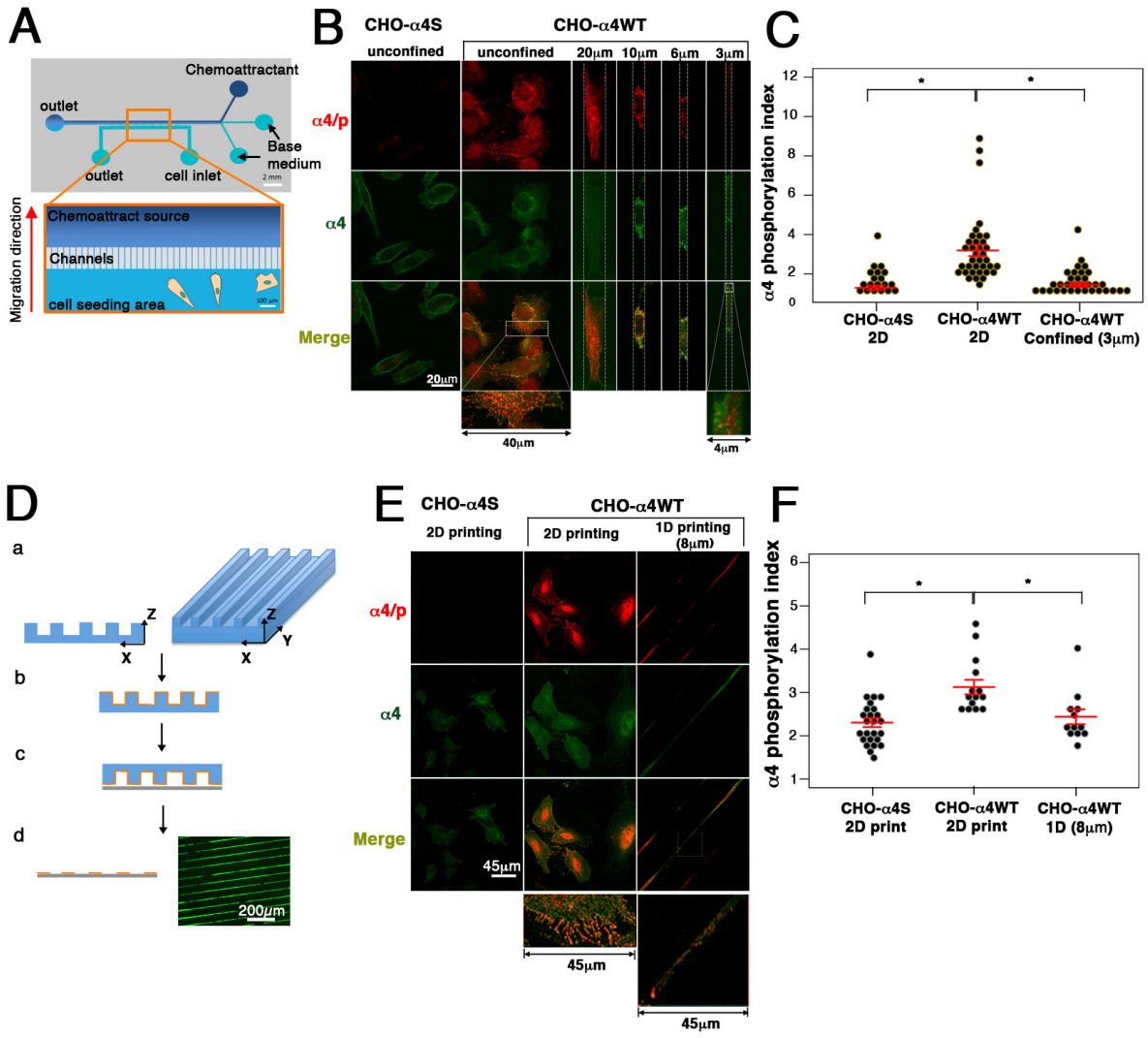

Figure 6-1. Effects of physical confinement on α4 phosphorylation. (A) Schematic of the microchannel device bounded to glass slide. Also shown below is a close-up detail of channel array. Channels of 50-μm, 20-μm, 10-μm, 6-μm, and 3-μm in width were used in the study. The red arrow (left to the close-up channel array) indicates the direction of migration. (B) CHO-α4WT and CHO-α4S988A cells were seeded in cell seeding area (indicated as unconfined) and then induced to migrate through 20-μm, 10-μm, 6-μm, or 3-μm fibronectin-coated channels. Cells expressing GFP-α4

integrins were stained with phosphorylated α4 (red) and imaged by dual color confocal microcopy. (C) For each designated condition, overall level of α4 phosphorylation is quantified by measuring α4 phosphorylation red fluorescence intensity normalized by GFP-tagged α4 integrin. (D) Schematic representation of microcontact printing. (a and b) PDMS stamp (blue) was coated with fibronectin (orange) to be printed. (c) Fibronectin was transferred by printing onto cover slide (gray) and then examined by fluorescence staining (d). (E) CHO-α4WT and CHO-α4S988A cells placed on either 2D or 1D fibronectin printed cover slide were stained with phosphorylated α4 and imaged by confocal microcopy (F) The overall α4 phosphorylation level was quantified by measuring α4 phosphorylation red fluorescence intensity normalized by GFP-tagged α4 integrin. Data represent means ± SEM. *, $P < 0.05$.

6.3.2 PKA activity of CHO-α4WT cells is reduced in response to physical confinement

It has reported that PKA (protein kinase A) is critical to regulate α4 integrin phosphorylation at Ser^{988} (Goldfinger et al., 2003) and α4 integrin functions as one of A Kinase Anchoring Proteins (AKAPs) recruiting PKA to cell membrane (Lim et al., 2007). Therefore we investigate if PKA is the upstream regulator modulating level of α4-phosphorylation in response to physical confinement. We evaluated compartmentalized PKA activity of CHO-α4WT cells in plasma membrane microdomains in unconfined or confined migration by using membrane-targeted fluorescence resonance energy transfer (FRET)-based A-Kinase Activity Reporters (AKARs-Kras) (Fig. 6-2A). This allows live-cell visualization of endogenous PKA activity dynamics with high spatiotemporal resolution. CHO-α4WT cells expressing AKAR4-Kras were first allowed to seed on cell seeding area and chemoattractant was applied to induce migration through 3μm channels. Time-lapse images demonstrate an overall reduction of PKA activity when CHO-α4WT cells transiting from unconfined to confined spaces (Fig. 6-3). In order to verify the effect of confinement on PKA activity, the PKA activity of CHO-α4WT cells in confined or unconfined spaces were first measured by quantifying the starting yellow-cyan emission ratio, followed by addition of PKA inhibitor, H89, for 30 minutes to detect the basal level of PKA activity (Fig. 6-2). The starting ratio of confined CHO-α4WT cells is significantly lower relative to unconfined cells (Fig. 6-2C). Moreover yellow-cyan emission ratios were plotted along with yellow intensities, displaying the non-correlation between emission ratio and transfection efficiency (Fig. 6-2D). Treating unconfined cells with 10μM H89 resulted in approximately 20% decrease of PKA activity and in contrast, confined cells treated with 10μM H89 results in

approximately 9% decrease of PKA activity (Fig. 6-2E). Therefore multiple lines of evidences together suggest that PKA activity of CHO-α4WT is reduced in confined spaces.

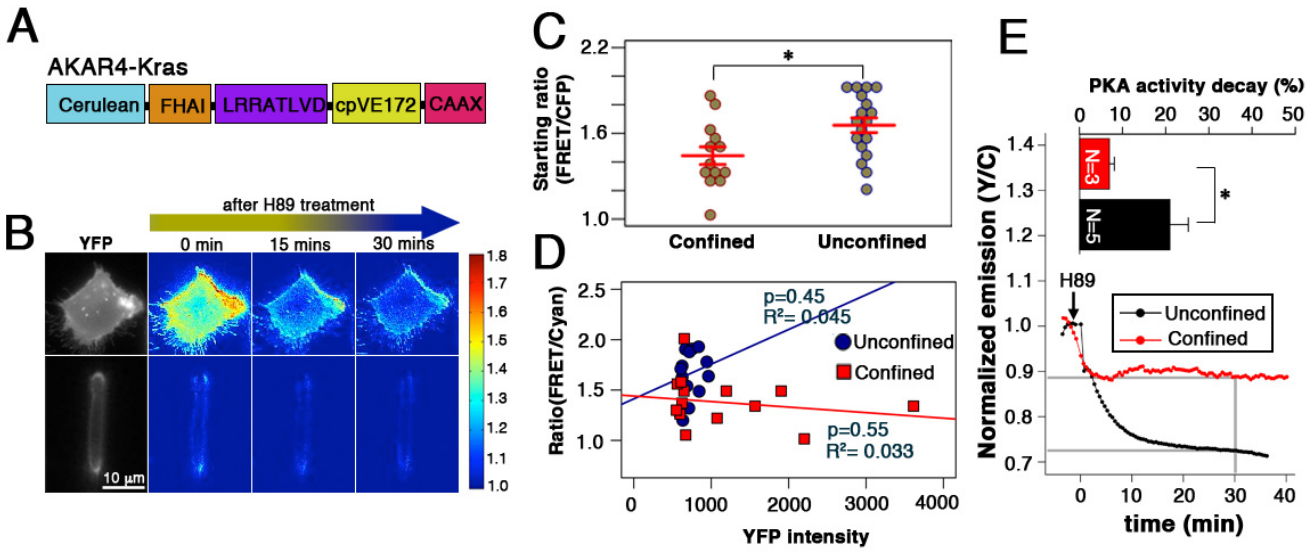

Figure 6-2 PKA activity is spatiotemporally modulated by physical confinement.

(A) Schematic representation of AKAR4-Kras (B) CHO-α4WT cells expressing AKAR4-Kras were plated on unconfined spaces or induced to 3μm channel to experience confinement. YFP images and ratiometric images of confined and unconfined cells before PKA inhibitor, H89, was added (0 min) and at 15 and 30 minute after the addition. (C) The initial PKA activity of confined or unconfined CHO-α4WT cell is quantified by measuring FRET to CFP emission ratio. Data presents means ± SEM. *, $P < 0.05$. (D) FRET to Cyan emission ratios of CHO-α4WT cells in confined and unconfined spaces are plotted with YFP intensity and data points are fitted with linear regression. Correlation coefficient, R^2 and p-value evaluating fitness are both displayed. (E) CHO-α4WT cells in confined (N=3) or unconfined (N=5) space were treated with 10μM H89 and the FRET to Cyan emission ratio was recorded every 30 seconds for 40 minutes. Bar graph displays the decaying percentage of PKA activity at 30 minute after addition of H89. Data presents means ± SEM. *, $P < 0.05$.

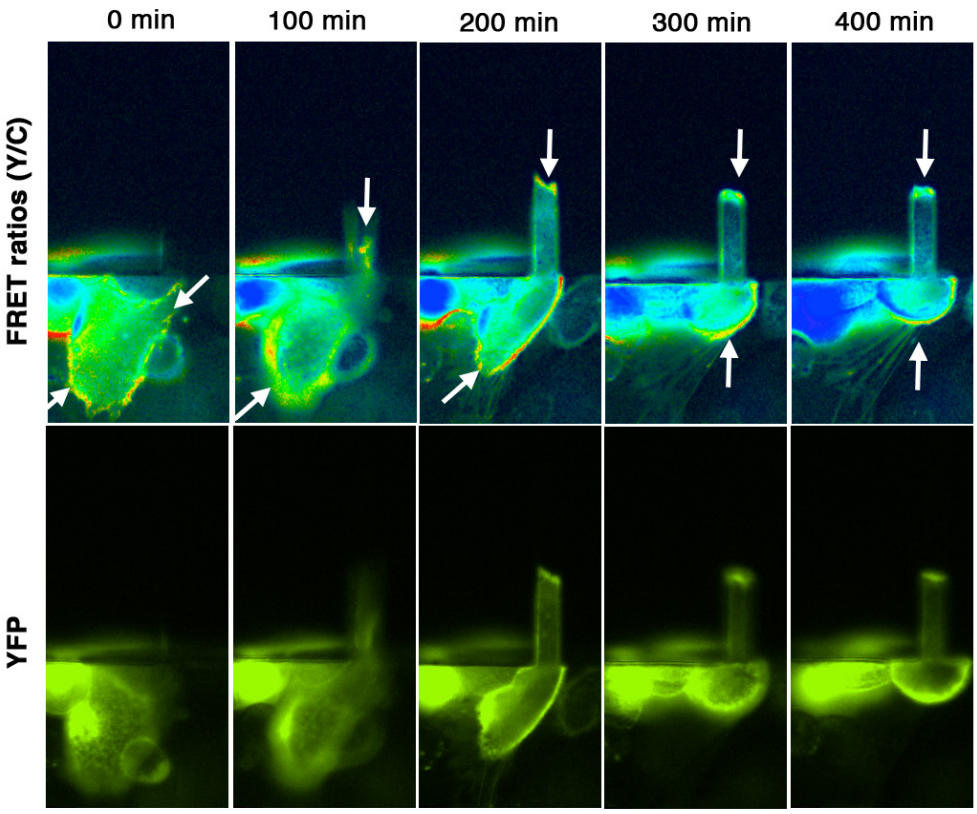

Figure 6-3. Change of spatiotemporal PKA activity of CHO-α4WT cells during migration transition between 2D surface and confinement. White arrows point leading and trailing edge of cell. Warmer color represents higher PKA activity.

6.3.3 Inhibiting and activating PKA activity of CHO-α4WT cells suppress unconfined and confined migration respectively

It has reported that phosphorylation of α4 cytoplasmic tail regulates Rac1 activation by inhibiting α4/paxillin binding(Liu et al., 1999; Nishiya et al., 2005). Moreover, we also found that the α4-mediated Rac1 activation is in the crosstalk with RhoA/myosin II pathway and it tightly regulates migration in response to different degree of confinement (Hung et al., 2013). Given that the level of α4 phosphorylation and PKA activity were both reduced as increasing degree of confinement, we sought to exanimate the effect of inhibiting or activating PKA on migration in unconfined versus confined spaces. CHO-α4WT cells were treated with PKA inducer, forskolin or PKA inhibitor, Rp-cAMPs and chemoattractant was then applied to induce migration through 20 μg/ml fibronectin-coated channel in width of 50μm, 20μm, 10μm, 6μm, and 3μm. CHO-α4WT cells treated with forskolin displayed a migration phenotype where cells migrated with high velocity in wide channels (50μm and 20μm) but with significantly lower migration velocity in narrow channel (6μm and 3μm), compared with vehicle control (Fig. 6-4A). In contrast, CHO-α4WT cells treated with Rp-cAMPs showed reverse phenotype to forskolin treatment. It demonstrates high migration velocity in narrow channels but significant lower migration velocity in wide channel (Fig. 6-4A). Because the α4 phosphorylation level of CHO-α4WT cells was reduced in both confined and 1D environments (Fig 6-1), we also tested CHO-α4WT cells migrating on 8μm-wide linear fibornectin line with the treatment of forskolin or Rp-cAMPs. Inhibiting and activating PKA activity promotes and suppresses 1D migration respectively in terms of velocity and instantaneous speed (Fig 6-4 D and E), which is similar to the phenotype of confined

migration. These data suggest that CHO-α4WT cells require reduced and elevated level of PKA activity to optimize confined and unconfined migration.

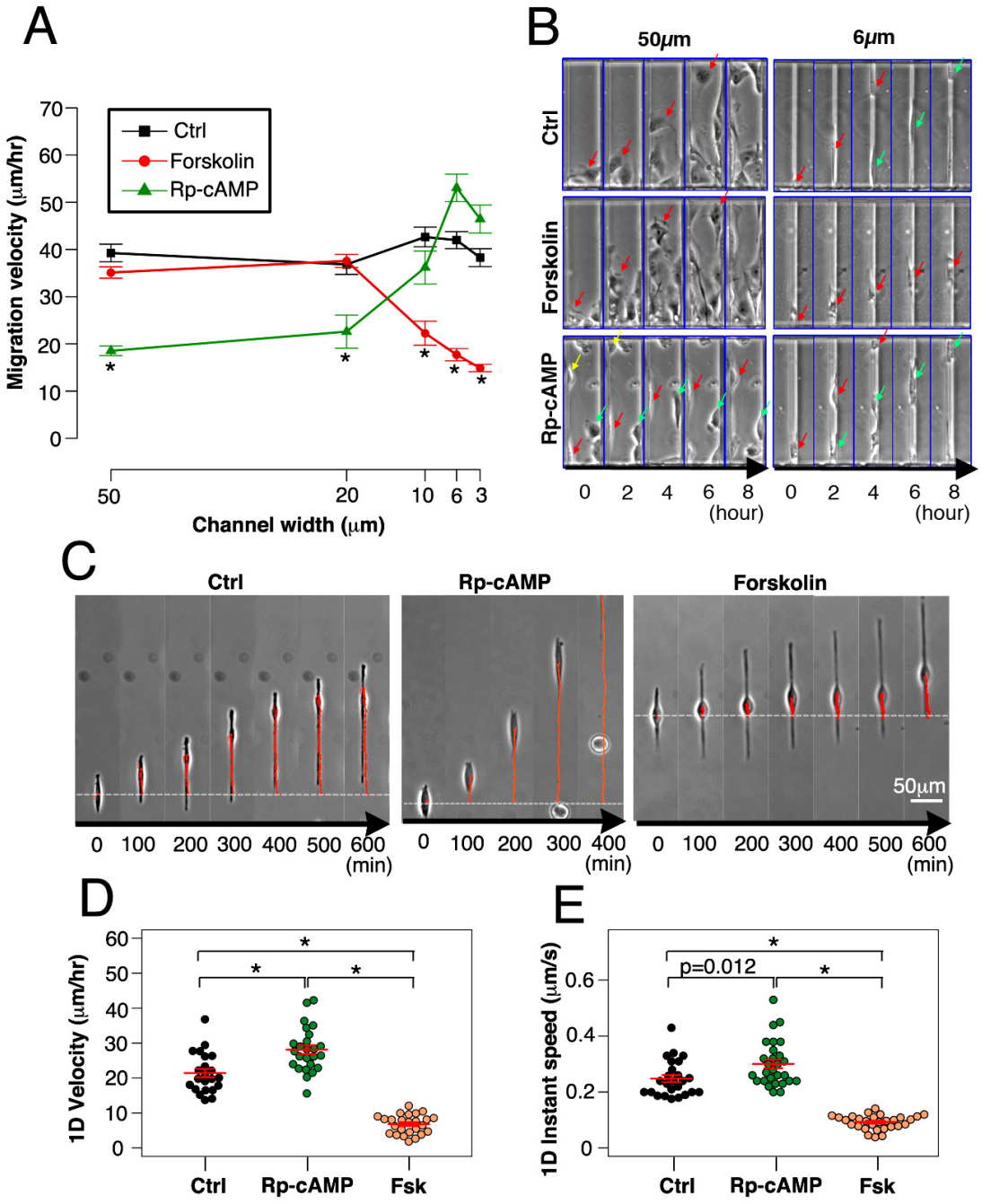

Figure 6-4. Effects of inhibiting or enhancing PKA activity on confined migration and 1D migration of CHO-α4WT cells. CHO-α4WT cells were treated with either PKA enhancer forskolin, PKA inhibitor Rp-cAMPs, or vehicle control and allowed to migrate inside of fibronectin-coated channel (A and B) or on fibronectin-

printed 8μm wide 1D pattern (C, D, and E). Their migration velocities (A and D) and instantaneous speed (E) were quantified. The time-lapse images of migrating cells in designated channel widths (B) and 1D pattern (C) are shown. Data represent means ± SEM. *, $P < 0.005$.

6.3.4 Activating or inhibiting PKA activity of CHO-α4WT regulates contractility and lamellipodia formation.

We have reported that CHO-α4WT cells regulate Rac1/myosin II crosstalk through α4-mediated signaling. CHO-α4S988A cells with phosphorylation point mutation at Ser^{988} cells displays smaller lamellipodia formation but higher densities of focal adhesion and stress fiber (Hung et al., 2013). In contrast the reversed phenotypes were observed in CHO-α4Y991A cells with α4/paxillin binding mutation(Hung et al., 2013). Because PKA is regulating α4-mediated signaling, it encourages us to test the effects of inhibiting or inducing PKA on focal adhesion and lamellipodia formation of CHO-α4WT cells. CHO-α4WT cells were first plated on fibornectin-coated 2D surface in the treatment of forskolin or Rp-cAMPs and stained stress fiber and paxillin were both imaged in each condition (Fig 6-5 A). Punctate structure of paxillin were identified and measured to determine the density of focal adhesion in designated condition (Fig. 6-5 B). Forskolin treated CHO-α4WT cells displayed lower density of focal adhesion but formed larger lamellipodia (Fig. 6-5 A, C, and D). In contrast, Rp-cAMPs treated CHO-α4WT cells has higher density in terms of the number of focal adhesion normalized by spreading area and total area of focal adhesion normalized by cell spreading area (Fig. 6-5A and C). However, the areas of cell spreading and lamellipodia formation of Rp-cAMPs treated CHO-α4WT cells were significantly smaller than those of vehicle control and forskolin treated CHO-α4WT cells (Fig. 6-5D). These results imply that the myosin II and protrusion activities of CHO-α4WT cells can be regulated by PKA activity.

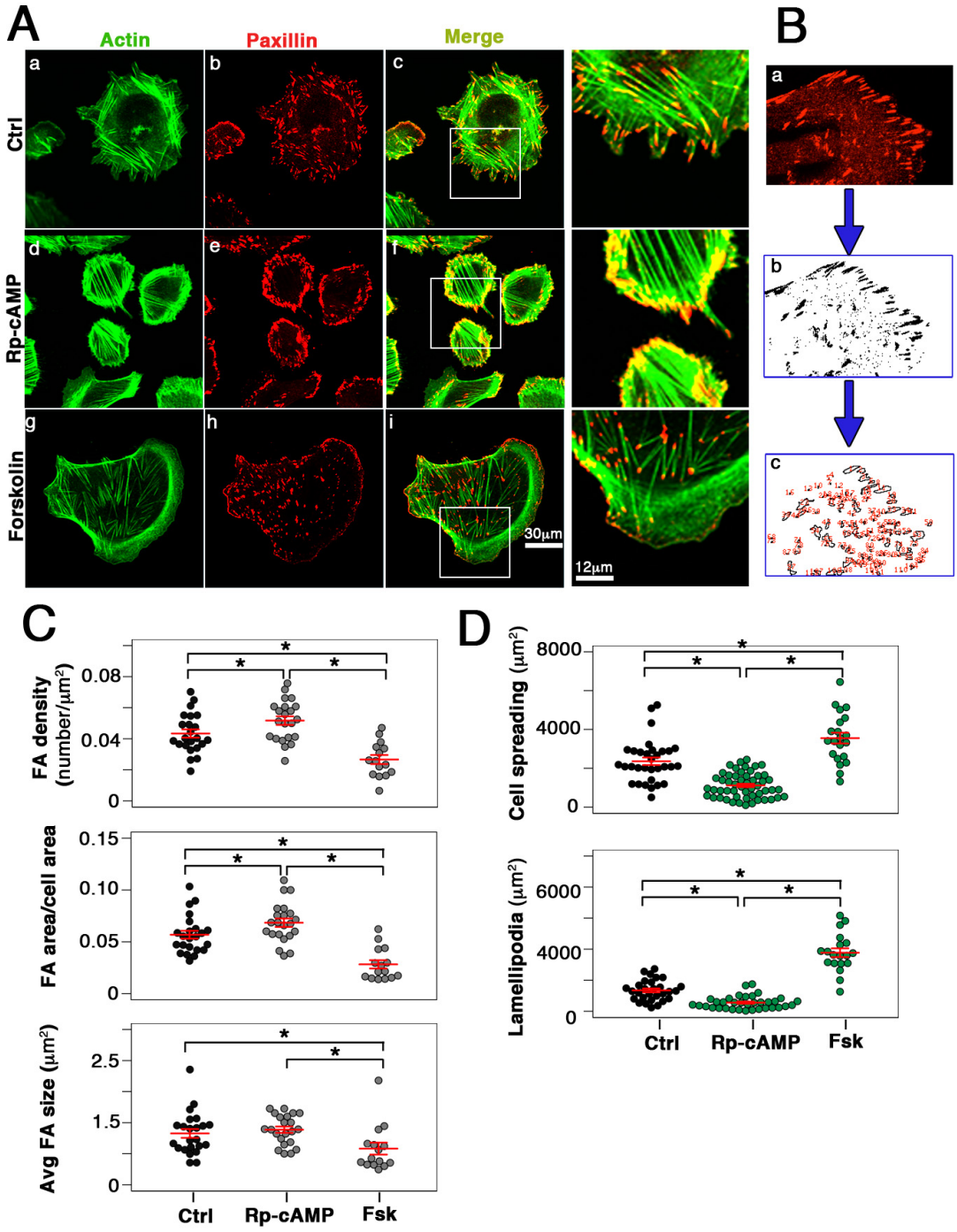

Figure 6-5. Effects of inducing or inhibiting PKA activity on focal adhesion densities and lamellipodia formation of CHO-α4WT cells on 2D surfaces. CHO-α4WT cells were plated on fibronectin-coated coverslips in presence of vehicle control, PKA inhibitor Rp-cAMPs, or PKA inducer forskolin. (A) Cells stained with phalloidin (green) and with an antibody against paxillin (red) were imaged by

confocal microcopy. Focal adhesion images (B, a) were first processed by background subtraction and binary conversion (B, b) and then identified and measured by imageJ software (B, c). Focal adhesion densities were evaluated as the number of focal adhesions (FA) per micrometer squared (C, a) or total area of focal adhesions normalized by cell spreading area (C, b) in designated conditions. Averaged focal adhesion areas within cells were also quantified (C, c). Cell spreading areas (D, a) and the area of lamellipodia protrusion (D, b) were quantified. Data represent means ± SEM. *, $P < 0.05$.

6.3.5 α4 and α5 amplify PKA signaling but not serve as mechanosenser to physical constraint.

It has reported that α4 and α5 integrins play the important role to induce PKA gradient in migration CHO cells (Lim et al., 2008). Other study also revealed that release of cAMP gating is mediated through α6β4 signaling pathway (O'Connor et al., 1998). Given the fact that integrins play the critical role in regulating cAMP and PKA activity, we next investigate if the reduced PKA of in confinement is resulted from integrins. We have evaluated PKA activity of three cell lines expressing α4 and α5 (CHO-α4WT cells), only α5 (CHO cells), and neither α4, α5, nor other integrins (CHO-B2)(Chen et al., 2012). Interestingly, we found that PKA activity is significantly reduced in 3μm channel in CHO-α4WT, CHO, and CHO-B2 cells, relative to cells on unconfined spaces (6-6 A). CHO-α4WT, CHO, and CHO-B2 display gradient from leading to trailing edges on 2D surface. In contrast, confined cells exhibit the elevated PKA activity in two ends of cell body (Fig 6-6 B).

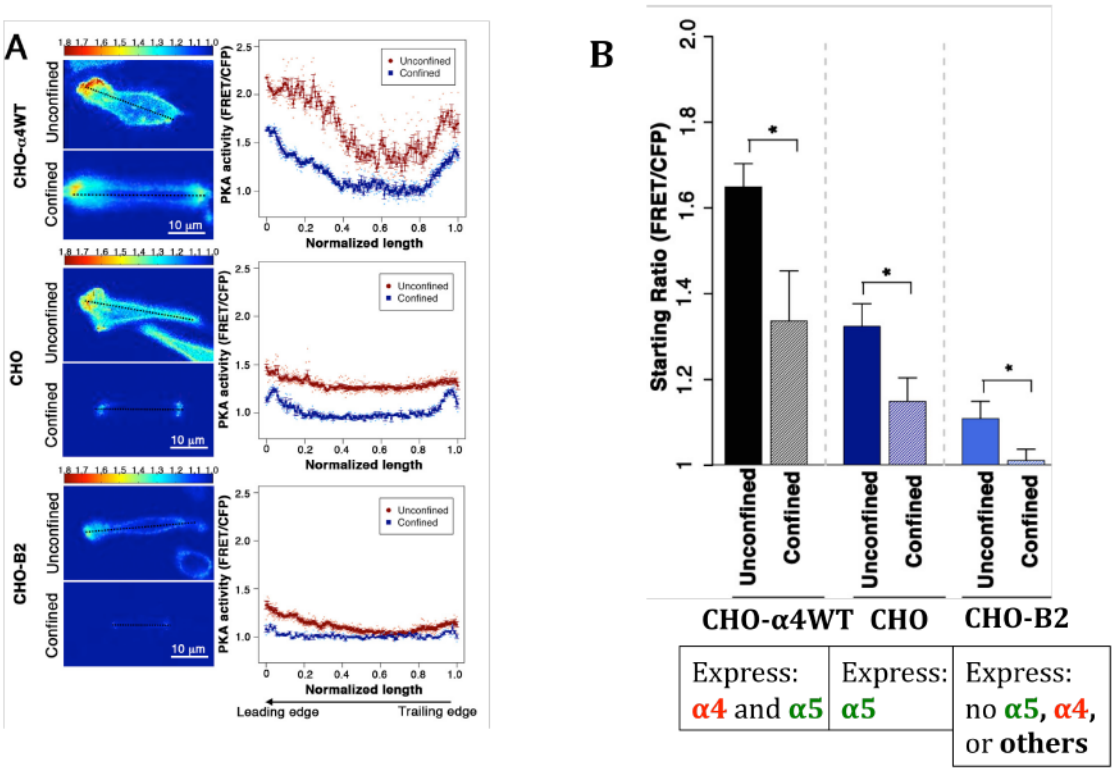

Fig. 6-6 comparison of PKA activity of CHO-α4WT, CHO, and CHO-B2 cell lines in unconfined versus confined spaces. (A) CHO-α4WT, CHO, or CHO-B2 cells expressing AKAR4-Kras were plated on unconfined spaces or induced to 3μm channel to experience confinement. Profile plots shown are the averaged ratiometric values for six line scans centered around the dashed tracing **(B)** The initial PKA activity of confined or unconfined cell is quantified by measuring FRET to CFP emission ratio. Data presents means ± SEM. *, $P < 0.05$.

CHAPTER 7

Concluding remarks

Our microchannel assay provides a systematic means to examine migratory behaviors in response to varying degrees of confinement, where the absence of confinement (wide channels where $W>d_{cell}$) mimics a 2D environment. This enables us to directly compare and contrast 2D versus confined migration in a quantitative manner, and to elucidate the mechanisms underlying these two regimes. Using this assay, we examined several fibroblast-like cell types expressing or lacking α4β1 integrin. Fibroblast-like cells, including the α4β1 integrin-expressing CHO cells and A375-SM cells, employ a 'mesenchymal mode' of migration on 2D surfaces, in which lamellipodia protrusion and cell-ECM adhesion play critical roles. In contrast, cells migrating through physically confined spaces display less extensive protrusive activity at the leading edge. This migration mode depends on myosin II-driven contractility, akin to amoeboid migration of T lymphocytes(Jacobelli et al., 2010; Yoshida and Soldati, 2006). Unlike lymphocytes, however, CHO-α4WT and A375-SM cells in narrow channels retain well-organized stress fibers, which are reminiscent of those observed in fibroblasts in a 3D linear elastic environment or under other forms of physical constraints (Doyle et al., 2009; Ghibaudo et al., 2009; Petrie et al., 2012). It is possible that in response to the physical constraints, fibroblast-like cells switch their migration mode to become more amoeboid-like while still retaining some mesenchymal characteristics; specific cell types may possess certain degrees of

mesenchymal or amoeboid characteristics. In response to confinement or other physical constraints, the cells may undergo different degrees of mesenchymal-to-amoeboid transition, during which the strategy for optimizing cell migration has to be altered. It can be envisioned that myosin II-driven contractility of fibroblast-like cells may facilitate confined migration by laterally constraining the cell body, thus minimizing cell-substrate contact interactions (Sixt, 2012). On the other hand, Rac1-dependent lamellipodia protrusion rather than the myosin II-driven contractility becomes more critical in 2D migration. To adapt to different degrees of confinement, the cells optimize the signaling network by adjusting the balance between Rac1 and myosin II activities.

The α4/paxillin-mediated signaling network **(Fig. 7-1)** provides a paradigm for such adaptation in response to altered physical environment. On a 2D surface, α4β1 integrin promotes the migration of CHO-α4WT cells by optimizing Rac1 activity at the cell front (Goldfinger et al., 2003). The elevated Rac1 activity is maintained by Ser^{988}-phosphorylation at the α4 cytoplasmic tail that prevents α4/paxillin binding. In contrast, as cells experience increasing degrees of confinement, α4/paxillin binding becomes progressively indispensible for effective migration. Therefore, the levels of α4/paxillin binding and Ser^{988}-phosphorylation are modulated as CHO-α4WT cells migrate in different microenvironments. The mechanism of this signaling adaptation in response to physical confinement is beyond the scope of this paper, but we can envision three possible mechanisms. First, Ser^{988}-phosphorylation and its downstream targets could be regulated via α4β1-ligand engagement, where α4β1 integrin functions as a mechanosensor. For instance, it has been reported that engagement of α4β1-specific ligand down-regulates RhoA and stress fiber formation in A375-SM cells plated on 2D surfaces (Moyano et al., 2003).

Although our data show that under confinement VCAM-1 is not required for CHO-α4WT and A375-SM cells to reach maximum migration velocities, ECM proteins, such as fibronectin, may be secreted by the cells over the course of the microchannel assay and/or deposited from the chemoattractant (FBS) source, thereby providing force signals. This opens a second possibility: other integrins or cell surface receptors may act as mechanosensors (Jalali et al., 2001; Li et al., 2002; Roca-Cusachs et al., 2012) that regulate the cellular responses to physical confinement. A third possible mechanism is that the cytoskeleton itself may function as a mechanosensor (Janmey and Weitz, 2004; Ren et al., 2009; Schwarz and Gardel, 2012). The actomyosin network may sense the mechanical cues generated by confinement-induced cell shape changes (McBeath et al., 2004), leading to the observed cellular responses.

We show that disrupting α4/paxillin binding in α4β1-expressing CHO and A375-SM cells inhibits myosin II-driven contractility, and this defect can be rescued by treating cells with a Rac1 inhibitor. Likewise, treatment of fibroblasts and CHO cells lacking α4β1 integrin with the Rac1 inhibitor augments migration in narrow channels by promoting myosin II-driven contractility. Moreover, blebbistatin increases migration velocity in wide channels via enhancement of Rac1 activity. We further show that the Rac1 inhibitor also has a rescue effect on primary $CD4^+$ T cells carrying the α4Y991A mutation, which is similar to that of CHO-α4WT and A375-SM cells under confinement. These observations support a crosstalk mechanism in which Rac1 and myosin II negatively regulate each other to modulate cell motility **(Fig. 7-1)**. Crosstalk between Rac1 and myosin II and vice versa has been reported by numerous studies (Burridge and Wennerberg, 2004; Bustos et al., 2008). Rac1 can inhibit myosin II-driven contractility by several mechanisms. For example, Rac1 can inhibit Rho by activating p190RhoGAP (Nimnual et al., 2003). Rac1 can also inhibit

myosin II activities by promoting phosphorylation of MLCK (Sanders et al., 1999) or myosin II heavy chain (Leeuwen et al., 1997) via PAK or by inhibiting phosphorylation of myosin II regulatory light chain via WAVE2 (Sanz-Moreno et al., 2008).

Our data reveal that MIIB but not MIIA is required for optimizing 2D migration, whereas this scenario is reversed for confined migration. These observations are in agreement with published data showing that MIIB and MIIA have overlapping but differential functions in cell migration. MIIA is required for stress fiber formation, cellular contractility and trailing edge retraction (Even-Ram et al., 2007; Sandquist et al., 2006; Vicente-Manzanares et al., 2011; Vicente-Manzanares et al., 2007). It has been proposed that MIIA is the predominant downstream target for the Rho pathway, which is based on observations showing that MIIA-depletion has similar effects as blebbistatin or Y-27632 treatment. Indeed, we also observed that MIIA-depletion had similar effects as inhibiting ROCK or the enzyme cycle of myosin II; all interventions impaired confined, but not 2D, migration, thus suggesting that MIIA-driven contractility is critical for the efficient migration of CHO-α4WT cells under physical confinement (**Fig. 7-1**). In contrast to MIIA, MIIB plays a relatively minor role in cellular contractility, as demonstrated by traction force measurements and stress fiber evaluations of MIIA- and MIIB-deficient mouse embryonic fibroblasts (Cai et al., 2006). Instead, MIIB stabilizes front-back polarity of migrating cells (Vicente-Manzanares et al., 2011; Vicente-Manzanares et al., 2007) and contributes to leading edge protrusion (Giannone et al., 2007). Consistent with these studies, we have shown that MIIB-depleted CHO-α4WT cells on 2D substrates exhibited a rounded morphology and polarity defects, which greatly inhibited 2D migration. However, this molecular intervention had little or no inhibitory effect on

confined migration. Inhibition of MLCK impairs the activation of both MIIA and MIIB, leading to reduced migration in both wide and narrow channels. This observation suggests that in wide channels MIIB-depletion may be dominant over the potential elevation of Rac1 induced by suppressed MIIA activity.

Altogether, the first part of study (Chapter 2, 3, 4 and 5) reveals that distinct mechanisms regulate cell migration in 2D versus confined spaces, which involves Rac1-myosin II crosstalk. The α4β1-mediated pathway provides a paradigm for the plasticity of cells in which a signaling network can be tuned in distinct manners in response to different physical conditions to achieve maximal cell motility. We then elucidated how the mechanical signals generated by physical confinement induce cellular responses and how cells alter their signaling strategies to optimize cell motility.

As described in Chapter 6, PKA phosphorylates α4 cytoplasmic tail and serves as upstream regulator to wide variety of enzyme. Our study has revealed that membrane-PKA activity was reduced when cells experience confinement, which is not resulted by α4β1 or α5β1 integrin expression. However, α4β1 and α5β1 integrin both enhances PKA gradient cross cell body in both confined and unconfined spaces. This implies that α4β1 and α5β1 can either promote or function as AKAPs in leading edge. Chemoattractant activates Rac1, in turns triggering the recruitment of actin nucleation protein Arp2/3 and WAVEs to facilitate net-like actin polymerization. Given that WAVEs, functioning AKAPs, localizes PKA to leading edge, therefore we hypothesize that for the cell doesn't express α4β1 integrins, PKA activity at the leading edge is first accomplished by actin nucleation (WAVEs) that is activated by chemoattractants. In regions away from the leading edge, Rac1 and myosin II are in balance due to lack of external signals. However, α4β1 integrins can amplify the

signaling of PKA activation by recruiting PKA to leading edge as AKAPs. PKA gradient is established by WAVEs but amplified by a4. In regions away from the leading edge, the balance between Rac1 and myosin II is broken by a4/paxillin that inhibits Rac1 and enhances myosin II.

In confinement, actin polymerization displays a bipolar pattern where also locates water channels, focal adhesion, and several types of integrin(Stroka et al., 2014). Confined cell demonstrates highly aligned structure of stress fiber, which connects to both ends of cell body (Hung et al., 2013). These evidences together imply that confined cells preferentially locate wide variety of molecules to the part exposed to open space. On the other hand, it has reported that filamentous actin serves in a mechano-sensitive capacity itself and compressive force prevents Arp2/3 from further actin polymerization (Risca et al., 2012). We can therefore suggest that reduced PKA activity in confined cells is possibly resulted from the limitation of actin polymerization against the wall where cytoskeleton associating AKAPs is prevented to develop.

It as been well studied that PKA phosphorylates RhoA on Ser188, leading to increased RhoGDI association and decreased RhoA signaling (Wong and Scott, 2004). PKA activation on AKAP-Lbs also inhibits Rho-GEF activity, thereby preventing the activation of RhoA (Wong and Scott, 2004). We have shown that the local PKA activity is reduced in confinement, which is possibly due to restricted spatial actin polymerization. Therefore RhoA/myosin II activity can elevate at the part where PKA is reduced. This phenomena support our initial point that in physical constraint, cell up-regulates RhoA/myosin activity to optimize confined migration by switching toward myosin II-driven migration mode. For α4-expressing cell lines, this PKA reduction likely enhances myosin II activity via α4/paxillin binding, thus

promoting confined migration speed in α4-expressing cell line as we have observed in Chapter 2.

A

	WT		Y991A		S988A	
	W	N	W	N	W	N
untreated	+++	+++	+++	+	+	+++
NSC23766	+	+++	+	+++	+	+++
Y-27632	+++	+	+++	+	+++	+
Blebb	+++	+	+++	+	+++	+

	WT	
	W	N
untreated	+++	+++
ML-7	+	+
Y-27632	+++	+
Blebb	+++	+
MIIA-KD	+++	+
MIIB-KD	+	+++

B

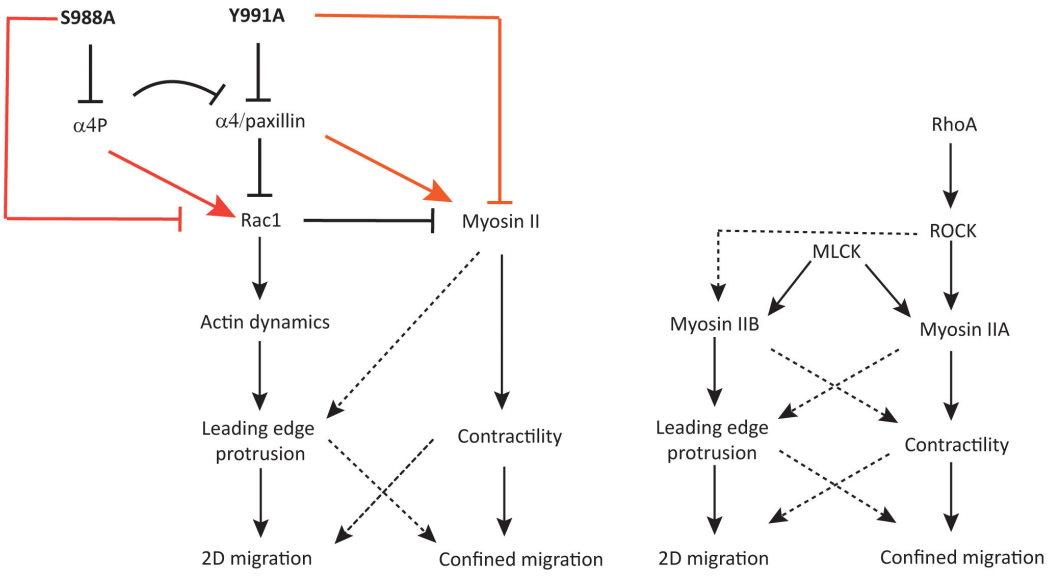

Figure 7-1 Model and summary of α4-tail-mediated signaling in optimizing 2D and confined migrations. **(A)** The tables summarize the effects of introducing the α4 tail mutations or various pharmacological inhibitors/siRNAs on the migration of α4 integrin-expressing CHO cells through wide (W) and narrow (N) channels. **(B)** Distinct signaling pathways regulate 2D versus confined migration. Black lines: primary pathway; orange lines: end result from several signaling steps; black dashed lines: involved but not required.

CHAPTER 8

Suggested future work

8.1 Evaluating effect of confinement on gene regulation in microarray analysis

It is well established that the nucleus plays an important role in mechanotransduction signaling where the process of biochemical signal propagation and processing, as most signaling pathways eventually culminate with nuclear proteins binding to specific genomic elements to modulate transcription. It is also known that the nucleus is mechanically connected to the rest of the cell via LINC (**Li**nker of **N**ucleoskeleton and **C**ytoskeleton) complex structures in the nuclear envelope(Chambliss et al., 2013). These complexes play similar role of focal adhesions at the plasma membrane, allowing for cytoskeletal and external forces to result in nuclear deformations. According to Greogory R. Fedorchak, nucleus deformation could result in change of expression level by altering the interaction between chromatin and nuclear lamina, calcium or other ion influx to nucleus, or force transmitted across the LINC protein to alter gene location(Wang et al., 2009a). In general, force-generated conformational change of protein at nucleus envelope or interior can expose the active site of protein, thus further facilitating interaction or phosphorylation of protein. Moreover, nowadays we know that chromosome, in nucleus, has high spatial specificity; deformation of nucleus could bring specific gene close to nucleus pore or active protein site of nucleus envelope or interior nucleus.

Given that cells in 1D substrate line and confinement have elongated nucleus morphology(Khatau et al., 2012), besides actin and myosin II, those speculated mechano-sensor as prescribed in prior chapters, the compression of nucleus could also likely induces regulation of gene expression by deforming the nucleus shape. We have maturely developed the method to purify sufficient quantity of m-RNA from confined cell on 1D pattern. This allows us to probe the modification of gene regulation of confined cell relative to unconfined cells via microarray analysis (Fig 8-1).

8.2 Evaluating the role of α4 integrin in metastatic potential of glioblastoma (GMB) in brain micro-vessel network.

Vascular cell adhesion molecule-1 (VCAM-1) is an endothelial cell membrane glycoprotein that has been implicated in leukocyte/endothelial cell interactions in inflammation. It has been reported that human brain micro-vessel (diameter: 5~10 μm) endothelial cells (HBMEC) expresses high level of VCAM-1. Symptoms of a glioblastoma multiform in adults includes seizures, paralysis of area of body, changes in behavior, memory, or thinking abilities. α4β1-expressing glioblastoma cell (GMB) migrates in brain through VCAM-1 expressing micro-vessel network (Fig. 8-2), which is akin to PDMS-based microchannel developed in our lab. Therefore it is critical to reveal if GMB metastasis can be inhibited through modulating α4 cytoplasmic signaling in terms of confined migration. In prior chapter, we have employed α4/paxillin inhibitor to inhibit confined migration of α4-expression melanoma cell (A375-SM), Jurkat T-cells and, CD^{4+} T-cells. Therefore, investigating if this α4/paxillin inhibitor could also prevent glioblasoma metastasis in brain composed of micro-vessel network with high VCAM-1 expression becomes an

important study. This study can first be performed in in-vitro PDMS-based microchannel assay, followed by the evaluation of the metastatic potential of glioblastroma cells migrating in brain tissue based on the conditions established in vitro. The results of this investigation will shed the light on potential cure of brain cancer metastasis.

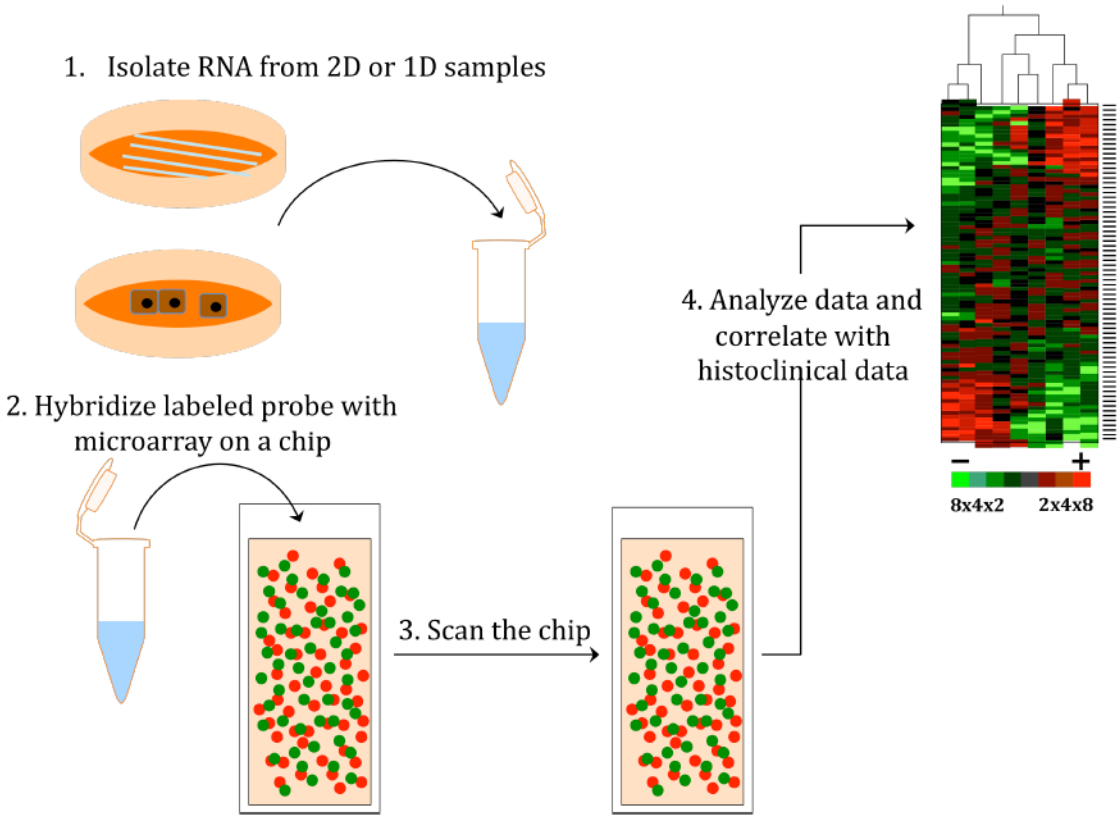

Figure 8-1 the procedure to evaluate gene regulation of confined (1D) and unconfined (2D) cells by using microarray technology.

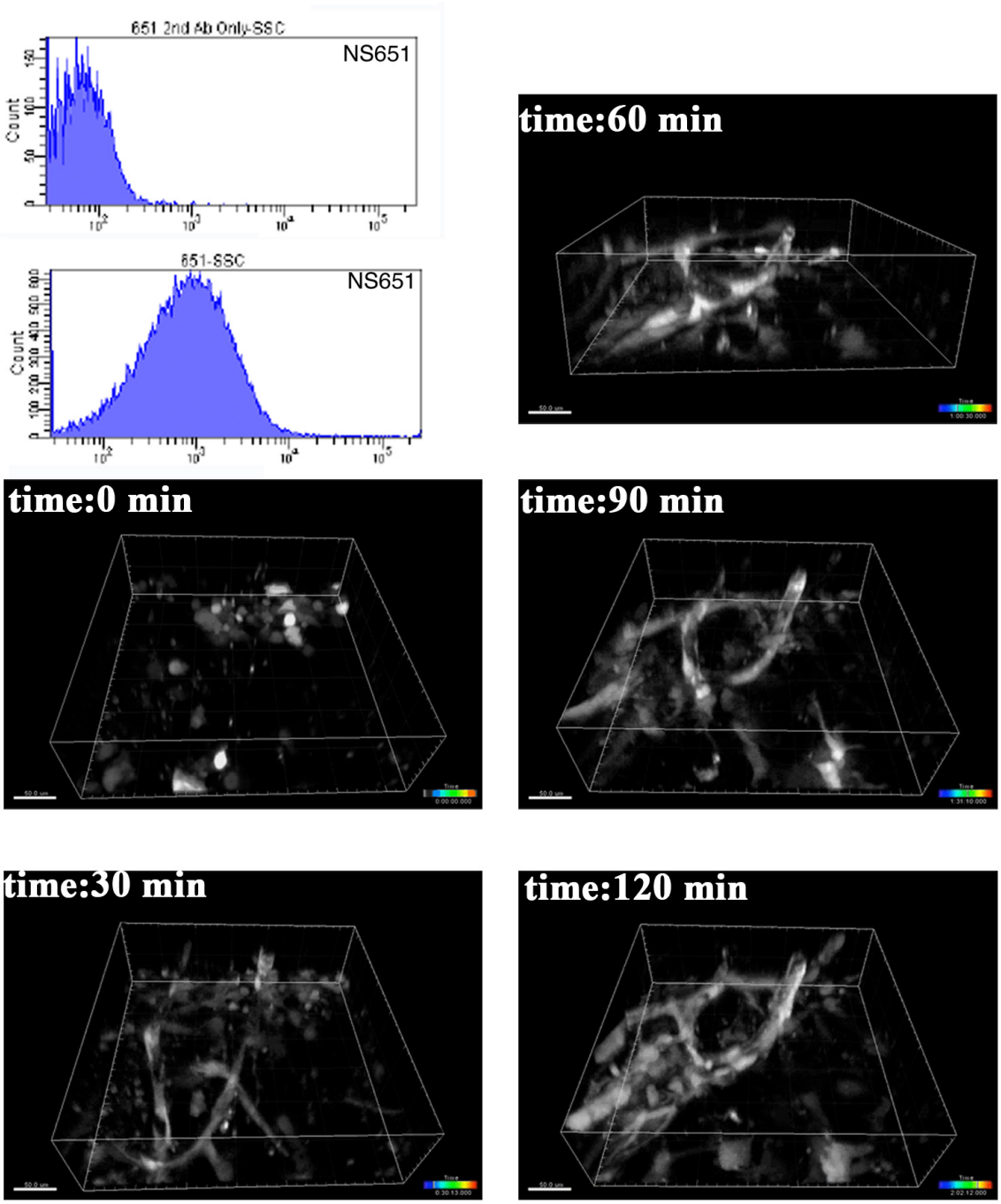

Figure 8-2. Metastasis of glioblastoma cells in mouse brain tissue. α4 expressing level of glioblastoma cell was evaluated by flow cytometry, relative to control (upright image). Time-lapse images demonstrate glioblastoma metastasis within micro-vessel of mouse brain tissue.

References Cited

Alexander, S., G.E. Koehl, M. Hirschberg, E.K. Geissler, and P. Friedl. 2008. Dynamic imaging of cancer growth and invasion: a modified skin-fold chamber model. *Histochem. Cell Biol.* 130:1147-1154.

Arthur, W.T., and K. Burridge. 2001. RhoA inactivation by p190RhoGAP regulates cell spreading and migration by promoting membrane protrusion and polarity. *Molecular biology of the cell*. 12:2711-2720.

Askari, J.A., C.J. Tynan, S.E. Webb, M.L. Martin-Fernandez, C. Ballestrem, and M.J. Humphries. 2010. Focal adhesions are sites of integrin extension. *The Journal of cell biology*. 188:891-903.

Backert, S., B. Kenny, R. Gerhard, N. Tegtmeyer, and S. Brandt. 2010. PKA-mediated phosphorylation of EPEC-Tir at serine residues 434 and 463: A novel pathway in regulating Rac1 GTPase function. *Gut microbes*. 1:94-99.

Balzer, E.M., Z. Tong, C.D. Paul, W.C. Hung, K.M. Stroka, A.E. Boggs, S.S. Martin, and K. Konstantopoulos. 2012. Physical confinement alters tumor cell adhesion and migration phenotypes. *FASEB J.* 26:4045-4056.

Brandt, S., B. Kenny, M. Rohde, N. Martinez-Quiles, and S. Backert. 2009. Dual infection system identifies a crucial role for PKA-mediated serine phosphorylation of the EPEC-Tir-injected effector protein in regulating Rac1 function. *Cellular microbiology*. 11:1254-1271.

Burridge, K., and K. Wennerberg. 2004. Rho and Rac take center stage. *Cell*. 116:167-179.

Bustos, R.I., M.A. Forget, J.E. Settleman, and S.H. Hansen. 2008. Coordination of Rho and Rac GTPase function via p190B RhoGAP. *Curr. Biol.* 18:1606-1611.

Cai, Y., N. Biais, G. Giannone, M. Tanase, G. Jiang, J.M. Hofman, C.H. Wiggins, P. Silberzan, A. Buguin, B. Ladoux, and M.P. Sheetz. 2006. Nonmuscle myosin IIA-dependent force inhibits cell spreading and drives F-actin flow. *Biophys. J.* 91:3907-3920.

Chambliss, A.B., S.B. Khatau, N. Erdenberger, D.K. Robinson, D. Hodzic, G.D. Longmore, and D. Wirtz. 2013. The LINC-anchored actin cap connects the extracellular milieu to the nucleus for ultrafast mechanotransduction. *Scientific reports*. 3:1087.

Chaw, K.C., M. Manimaran, F.E. Tay, and S. Swaminathan. 2007. Matrigel coated polydimethylsiloxane based microfluidic devices for studying metastatic and non-metastatic cancer cell invasion and migration. *Biomedical microdevices*. 9:597-602.

Chen, L., M. Vicente-Manzanares, L. Potvin-Trottier, P.W. Wiseman, and A.R. Horwitz. 2012. The integrin-ligand interaction regulates adhesion and migration through a molecular clutch. *PLoS One*. 7:e40202.

Chen, S.H., W.C. Hung, P. Wang, C. Paul, and K. Konstantopoulos. 2013. Mesothelin binding to CA125/MUC16 promotes pancreatic cancer cell motility and invasion via MMP-7 activation. *Scientific reports*. 3:1870.

Chrzanowska-Wodnicka, M., and K. Burridge. 1996. Rho-stimulated contractility drives the formation of stress fibers and focal adhesions. *J. Cell Biol.* 133:1403-1415.

Dikeman, D.A., L.A. Rivera Rosado, T.A. Horn, C.S. Alves, K. Konstantopoulos, and J.T. Yang. 2008. alpha4 beta1-Integrin regulates directionally persistent cell migration in response to shear flow stimulation. *American journal of physiology. Cell physiology*. 295:C151-159.

DiMilla, P.A., J.A. Stone, J.A. Quinn, S.M. Albelda, and D.A. Lauffenburger. 1993. Maximal migration of human smooth muscle cells on fibronectin and type IV collagen occurs at an intermediate attachment strength. *J Cell Biol*. 122:729-737.

Doyle, A.D., F.W. Wang, K. Matsumoto, and K.M. Yamada. 2009. One-dimensional topography underlies three-dimensional fibrillar cell migration. *The Journal of cell biology*. 184:481-490.

Even-Ram, S., A.D. Doyle, M.A. Conti, K. Matsumoto, R.S. Adelstein, and K.M. Yamada. 2007. Myosin IIA regulates cell motility and actomyosin-microtubule crosstalk. *Nature cell biology*. 9:299-309.

Feral, C.C., D.M. Rose, J. Han, N. Fox, G.J. Silverman, K. Kaushansky, and M.H. Ginsberg. 2006. Blocking the alpha 4 integrin-paxillin interaction selectively impairs mononuclear leukocyte recruitment to an inflammatory site. *J. Clin. Invest.* 116:715-723.

Friedl, P., and S. Alexander. 2011. Cancer Invasion and the Microenvironment: Plasticity and Reciprocity. *Cell*. 147:992-1009.

Friedl, P., and E.B. Brocker. 2000. T cell migration in three-dimensional extracellular matrix: guidance by polarity and sensations. *Developmental immunology*. 7:249-266.

Friedl, P., F. Entschladen, C. Conrad, B. Niggemann, and K.S. Zanker. 1998. CD4+ T lymphocytes migrating in three-dimensional collagen lattices lack focal

adhesions and utilize beta1 integrin-independent strategies for polarization, interaction with collagen fibers and locomotion. *European journal of immunology*. 28:2331-2343.

Gallo, G. 2006. RhoA-kinase coordinates F-actin organization and myosin II activity during semaphorin-3A-induced axon retraction. *J Cell Sci*. 119:3413-3423.

Ghibaudo, M., L. Trichet, J. Le Digabel, A. Richert, P. Hersen, and B. Ladoux. 2009. Substrate topography induces a crossover from 2D to 3D behavior in fibroblast migration. *Biophys. J.* 97:357-368.

Giannone, G., B.J. Dubin-Thaler, O. Rossier, Y. Cai, O. Chaga, G. Jiang, W. Beaver, H.G. Dobereiner, Y. Freund, G. Borisy, and M.P. Sheetz. 2007. Lamellipodial actin mechanically links myosin activity with adhesion-site formation. *Cell*. 128:561-575.

Goldfinger, L.E., J. Han, W.B. Kiosses, A.K. Howe, and M.H. Ginsberg. 2003. Spatial restriction of alpha4 integrin phosphorylation regulates lamellipodial stability and alpha4beta1-dependent cell migration. *The Journal of cell biology*. 162:731-741.

Gretz, J.E., A.O. Anderson, and S. Shaw. 1997. Cords, channels, corridors and conduits: critical architectural elements facilitating cell interactions in the lymph node cortex. *Immunological reviews*. 156:11-24.

Guilluy, C., R. Garcia-Mata, and K. Burridge. 2011. Rho protein crosstalk: another social network? *Trends Cell Biol.* 21:718-726.

Gunzer, M., A. Schafer, S. Borgmann, S. Grabbe, K.S. Zanker, E.B. Brocker, E. Kampgen, and P. Friedl. 2000. Antigen presentation in extracellular

matrix: interactions of T cells with dendritic cells are dynamic, short lived, and sequential. *Immunity*. 13:323-332.

Han, J., S. Liu, D.M. Rose, D.D. Schlaepfer, H. McDonald, and M.H. Ginsberg. 2001. Phosphorylation of the integrin alpha 4 cytoplasmic domain regulates paxillin binding. *J. Biol. Chem.* 276:40903-40909.

Hauzenberger, D., J. Klominek, S.E. Bergstrom, and K.G. Sundqvist. 1995. T lymphocyte migration: the influence of interactions via adhesion molecules, the T cell receptor, and cytokines. *Critical reviews in immunology*. 15:285-316.

Hung, W.C., S.H. Chen, C.D. Paul, K.M. Stroka, Y.C. Lo, J.T. Yang, and K. Konstantopoulos. 2013. Distinct signaling mechanisms regulate migration in unconfined versus confined spaces. *The Journal of cell biology*. 202:807-824.

Huttenlocher, A., and A.R. Horwitz. 2011. Integrins in cell migration. *Cold Spring Harbor perspectives in biology*. 3:a005074.

Jacobelli, J., R.S. Friedman, M.A. Conti, A.M. Lennon-Dumenil, M. Piel, C.M. Sorensen, R.S. Adelstein, and M.F. Krummel. 2010. Confinement-optimized three-dimensional T cell amoeboid motility is modulated via myosin IIA-regulated adhesions. *Nature immunology*. 11:953-961.

Jalali, S., M.A. del Pozo, K. Chen, H. Miao, Y. Li, M.A. Schwartz, J.Y. Shyy, and S. Chien. 2001. Integrin-mediated mechanotransduction requires its dynamic interaction with specific extracellular matrix (ECM) ligands. *Proc. Natl. Acad. Sci. U. S. A.* 98:1042-1046.

Janmey, P.A., and D.A. Weitz. 2004. Dealing with mechanics: mechanisms of force transduction in cells. *Trends Biochem. Sci.* 29:364-370.

Kelley, C.A., J.R. Sellers, D.L. Gard, D. Bui, R.S. Adelstein, and I.C. Baines. 1996. Xenopus nonmuscle myosin heavy chain isoforms have different subcellular localizations and enzymatic activities. *J. Cell Biol.* 134:675-687.

Khatau, S.B., R.J. Bloom, S. Bajpai, D. Razafsky, S. Zang, A. Giri, P.H. Wu, J. Marchand, A. Celedon, C.M. Hale, S.X. Sun, D. Hodzic, and D. Wirtz. 2012. The distinct roles of the nucleus and nucleus-cytoskeleton connections in three-dimensional cell migration. *Scientific reports*. 2:488.

Knight, B., C. Laukaitis, N. Akhtar, N.A. Hotchin, M. Edlund, and A.R. Horwitz. 2000. Visualizing muscle cell migration in situ. *Current biology : CB*. 10:576-585.

Kolega, J. 2006. The role of myosin II motor activity in distributing myosin asymmetrically and coupling protrusive activity to cell translocation. *Molecular biology of the cell*. 17:4435-4445.

Konstantopoulos, K., P.H. Wu, and D. Wirtz. 2013. Dimensional control of cancer cell migration. *Biophys. J.* 104:279-280.

Kreis, S., H.J. Schonfeld, C. Melchior, B. Steiner, and N. Kieffer. 2005. The intermediate filament protein vimentin binds specifically to a recombinant integrin alpha2/beta1 cytoplasmic tail complex and co-localizes with native alpha2/beta1 in endothelial cell focal adhesions. *Experimental cell research*. 305:110-121.

Kummer, C., B.G. Petrich, D.M. Rose, and M.H. Ginsberg. 2010. A small molecule that inhibits the interaction of paxillin and alpha 4 integrin inhibits accumulation of mononuclear leukocytes at a site of inflammation. *J. Biol. Chem.* 285:9462-9469.

Lee, C.S., C.K. Choi, E.Y. Shin, M.A. Schwartz, and E.G. Kim. 2010. Myosin II directly binds and inhibits Dbl family guanine nucleotide exchange factors: a possible link to Rho family GTPases. *The Journal of cell biology*. 190:663-674.

Leeuwen, F.N., H.E. Kain, R.A. Kammen, F. Michiels, O.W. Kranenburg, and J.G. Collard. 1997. The guanine nucleotide exchange factor Tiam1 affects neuronal morphology; opposing roles for the small GTPases Rac and Rho. *J. Cell Biol.* 139:797-807.

Leppert, D., S.L. Hauser, J.L. Kishiyama, S. An, L. Zeng, and E.J. Goetzl. 1995. Stimulation of matrix metalloproteinase-dependent migration of T cells by eicosanoids. *FASEB J*. 9:1473-1481.

Li, S., P. Butler, Y. Wang, Y. Hu, D.C. Han, S. Usami, J.L. Guan, and S. Chien. 2002. The role of the dynamics of focal adhesion kinase in the mechanotaxis of endothelial cells. *Proc. Natl. Acad. Sci. U. S. A.* 99:3546-3551.

Li, T., Y. Fang, G. Yang, J. Xu, Y. Zhu, and L. Liu. 2011. Effects of the balance in activity of RhoA and Rac1 on the shock-induced biphasic change of vascular reactivity in rats. *Annals of surgery*. 253:185-193.

Liao, J.K., M. Seto, and K. Noma. 2007. Rho kinase (ROCK) inhibitors. *J. Cardiovasc. Pharmacol.* 50:17-24.

Liddington, R.C., and M.H. Ginsberg. 2002. Integrin activation takes shape. *The Journal of cell biology*. 158:833-839.

Lim, C.J., J. Han, N. Yousefi, Y. Ma, P.S. Amieux, G.S. McKnight, S.S. Taylor, and M.H. Ginsberg. 2007. Alpha4 integrins are type I cAMP-dependent protein kinase-anchoring proteins. *Nature cell biology*. 9:415-421.

Lim, C.J., K.H. Kain, E. Tkachenko, L.E. Goldfinger, E. Gutierrez, M.D. Allen, A. Groisman, J. Zhang, and M.H. Ginsberg. 2008. Integrin-mediated protein kinase A activation at the leading edge of migrating cells. *Molecular biology of the cell*. 19:4930-4941.

Limouze, J., A.F. Straight, T. Mitchison, and J.R. Sellers. 2004. Specificity of blebbistatin, an inhibitor of myosin II. *J. Muscle Res. Cell Motil.* 25:337-341.

Liu, S., S.M. Thomas, D.G. Woodside, D.M. Rose, W.B. Kiosses, M. Pfaff, and M.H. Ginsberg. 1999. Binding of paxillin to alpha4 integrins modifies integrin-dependent biological responses. *Nature*. 402:676-681.

Mach, F., U. Schonbeck, R.P. Fabunmi, C. Murphy, E. Atkinson, J.Y. Bonnefoy, P. Graber, and P. Libby. 1999. T lymphocytes induce endothelial cell matrix metalloproteinase expression by a CD40L-dependent mechanism: implications for tubule formation. *The American journal of pathology*. 154:229-238.

Matsuura, N., W. Puzon-McLaughlin, A. Irie, Y. Morikawa, K. Kakudo, and Y. Takada. 1996. Induction of experimental bone metastasis in mice by transfection of integrin alpha 4 beta 1 into tumor cells. *Am. J. Pathol.* 148:55-61.

McBeath, R., D.M. Pirone, C.M. Nelson, K. Bhadriraju, and C.S. Chen. 2004. Cell shape, cytoskeletal tension, and RhoA regulate stem cell lineage commitment. *Developmental cell*. 6:483-495.

Mostafavi-Pour, Z., J.A. Askari, S.J. Parkinson, P.J. Parker, T.T. Ng, and M.J. Humphries. 2003. Integrin-specific signaling pathways controlling focal adhesion formation and cell migration. *J. Cell Biol.* 161:155-167.

Moyano, J.V., A. Maqueda, B. Casanova, and A. Garcia-Pardo. 2003. Alpha4beta1 integrin/ligand interaction inhibits alpha5beta1-induced stress fibers and focal adhesions via down-regulation of RhoA and induces melanoma cell migration. *Molecular biology of the cell*. 14:3699-3715.

Newell-Litwa, K.A., and A.R. Horwitz. 2011. Cell migration: PKA and RhoA set the pace. *Current biology : CB*. 21:R596-598.

Nimnual, A.S., L.J. Taylor, and D. Bar-Sagi. 2003. Redox-dependent downregulation of Rho by Rac. *Nat Cell Biol*. 5:236-241.

Nishiwaki, K., N. Hisamoto, and K. Matsumoto. 2000. A metalloprotease disintegrin that controls cell migration in Caenorhabditis elegans. *Science*. 288:2205-2208.

Nishiya, N., W.B. Kiosses, J. Han, and M.H. Ginsberg. 2005. An alpha4 integrin-paxillin-Arf-GAP complex restricts Rac activation to the leading edge of migrating cells. *Nature cell biology*. 7:343-352.

O'Connor, K.L., L.M. Shaw, and A.M. Mercurio. 1998. Release of cAMP gating by the alpha6beta4 integrin stimulates lamellae formation and the chemotactic migration of invasive carcinoma cells. *The Journal of cell biology*. 143:1749-1760.

Pasapera, A.M., I.C. Schneider, E. Rericha, D.D. Schlaepfer, and C.M. Waterman. 2010. Myosin II activity regulates vinculin recruitment to focal adhesions through FAK-mediated paxillin phosphorylation. *J. Cell Biol.* 188:877-890.

Pathak, A., and S. Kumar. 2012. Independent regulation of tumor cell migration by matrix stiffness and confinement. *Proc. Natl. Acad. Sci. U. S. A.* 109:10334-10339.

Petrie, R.J., N. Gavara, R.S. Chadwick, and K.M. Yamada. 2012. Nonpolarized signaling reveals two distinct modes of 3D cell migration. *J. Cell Biol.* 197:439-455.

Pinco, K.A., W. He, and J.T. Yang. 2002. alpha4beta1 integrin regulates lamellipodia protrusion via a focal complex/focal adhesion-independent mechanism. *Molecular biology of the cell*. 13:3203-3217.

Pollard, T.D. 2007. Regulation of actin filament assembly by Arp2/3 complex and formins. *Annual review of biophysics and biomolecular structure*. 36:451-477.

Ren, Y., J.C. Effler, M. Norstrom, T. Luo, R.A. Firtel, P.A. Iglesias, R.S. Rock, and D.N. Robinson. 2009. Mechanosensing through cooperative interactions between myosin II and the actin crosslinker cortexillin I. *Curr. Biol.* 19:1421-1428.

Risca, V.I., E.B. Wang, O. Chaudhuri, J.J. Chia, P.L. Geissler, and D.A. Fletcher. 2012. Actin filament curvature biases branching direction. *Proc Natl Acad Sci U S A*. 109:2913-2918.

Rivera Rosado, L.A., T.A. Horn, S.C. McGrath, R.J. Cotter, and J.T. Yang. 2011. Association between alpha4 integrin cytoplasmic tail and non-muscle myosin IIA regulates cell migration. *J. Cell Sci.* 124:483-492.

Roca-Cusachs, P., T. Iskratsch, and M.P. Sheetz. 2012. Finding the weakest link: exploring integrin-mediated mechanical molecular pathways. *J. Cell Sci.* 125:3025-3038.

Ryu, B., D.S. Kim, A.M. Deluca, and R.M. Alani. 2007. Comprehensive expression profiling of tumor cell lines identifies molecular signatures of melanoma progression. *PloS one*. 2:e594.

Sanders, L.C., F. Matsumura, G.M. Bokoch, and P. de Lanerolle. 1999. Inhibition of myosin light chain kinase by p21-activated kinase. *Science*. 283:2083-2085.

Sandquist, J.C., K.I. Swenson, K.A. Demali, K. Burridge, and A.R. Means. 2006. Rho kinase differentially regulates phosphorylation of nonmuscle myosin II isoforms A and B during cell rounding and migration. *J Biol Chem*. 281:35873-35883.

Sanz-Moreno, V., G. Gadea, J. Ahn, H. Paterson, P. Marra, S. Pinner, E. Sahai, and C.J. Marshall. 2008. Rac activation and inactivation control plasticity of tumor cell movement. *Cell*. 135:510-523.

Schwarz, U.S., and M.L. Gardel. 2012. United we stand: integrating the actin cytoskeleton and cell-matrix adhesions in cellular mechanotransduction. *J. Cell Sci.* 125:3051-3060.

Sixt, M. 2012. Cell migration: fibroblasts find a new way to get ahead. *J. Cell Biol.* 197:347-349.

Springer, T.A. 1994. Traffic signals for lymphocyte recirculation and leukocyte emigration: the multistep paradigm. *Cell*. 76:301-314.

Stetler-Stevenson, W.G., S. Aznavoorian, and L.A. Liotta. 1993. Tumor cell interactions with the extracellular matrix during invasion and metastasis. *Annual review of cell biology*. 9:541-573.

Stossel, T.P. 1994. The E. Donnall Thomas Lecture, 1993. The machinery of blood cell movements. *Blood*. 84:367-379.

Stroka, K.M., and H. Aranda-Espinoza. 2011. Endothelial cell substrate stiffness influences neutrophil transmigration via myosin light chain kinase-dependent cell contraction. *Blood*. 118:1632-1640.

Stroka, K.M., H. Jiang, S.H. Chen, Z. Tong, D. Wirtz, S.X. Sun, and K. Konstantopoulos. 2014. Water permeation drives tumor cell migration in confined microenvironments. *Cell*. 157:611-623.

Stroka, K.M., J.A. Vaitkus, and H. Aranda-Espinoza. 2012. Endothelial cells undergo morphological, biomechanical, and dynamic changes in response to tumor necrosis factor-alpha. *Eur. Biophys. J.* 41:939-947.

Tong, Z., E.M. Balzer, M.R. Dallas, W.C. Hung, K.J. Stebe, and K. Konstantopoulos. 2012a. Chemotaxis of cell populations through confined spaces at single-cell resolution. *PLoS One*. 7:e29211.

Tong, Z., L.S. Cheung, K.J. Stebe, and K. Konstantopoulos. 2012b. Selectin-mediated adhesion in shear flow using micropatterned substrates: multiple-bond interactions govern the critical length for cell binding. *Integrative biology : quantitative biosciences from nano to macro*. 4:847-856.

Totsukawa, G., Y. Yamakita, S. Yamashiro, D.J. Hartshorne, Y. Sasaki, and F. Matsumura. 2000. Distinct roles of ROCK (Rho-kinase) and MLCK in spatial regulation of MLC phosphorylation for assembly of stress fibers and focal adhesions in 3T3 fibroblasts. *The Journal of cell biology*. 150:797-806.

Urbano, J.M., P. Dominguez-Gimenez, B. Estrada, and M.D. Martin-Bermudo. 2011. PS integrins and laminins: key regulators of cell migration during Drosophila embryogenesis. *PLoS One*. 6:e23893.

Vicente-Manzanares, M., X. Ma, R.S. Adelstein, and A.R. Horwitz. 2009. Non-muscle myosin II takes centre stage in cell adhesion and migration. *Nature reviews. Molecular cell biology*. 10:778-790.

Vicente-Manzanares, M., K. Newell-Litwa, A.I. Bachir, L.A. Whitmore, and A.R. Horwitz. 2011. Myosin IIA/IIB restrict adhesive and protrusive signaling to generate front-back polarity in migrating cells. *J. Cell Biol.* 193:381-396.

Vicente-Manzanares, M., J. Zareno, L. Whitmore, C.K. Choi, and A.F. Horwitz. 2007. Regulation of protrusion, adhesion dynamics, and polarity by myosins IIA and IIB in migrating cells. *The Journal of cell biology*. 176:573-580.

von Andrian, U.H., and B. Engelhardt. 2003. Alpha4 integrins as therapeutic targets in autoimmune disease. *The New England journal of medicine*. 348:68-72.

Wang, N., J.D. Tytell, and D.E. Ingber. 2009a. Mechanotransduction at a distance: mechanically coupling the extracellular matrix with the nucleus. *Nature reviews. Molecular cell biology*. 10:75-82.

Wang, Y., X.R. Zheng, N. Riddick, M. Bryden, W. Baur, X. Zhang, and H.K. Surks. 2009b. ROCK isoform regulation of myosin phosphatase and contractility in vascular smooth muscle cells. *Circulation research*. 104:531-540.

Wilkinson, S., H.F. Paterson, and C.J. Marshall. 2005. Cdc42-MRCK and Rho-ROCK signalling cooperate in myosin phosphorylation and cell invasion. *Nature cell biology*. 7:255-261.

Wolf, K., S. Alexander, V. Schacht, L.M. Coussens, U.H. von Andrian, J. van Rheenen, E. Deryugina, and P. Friedl. 2009. Collagen-based cell migration models in vitro and in vivo. *Semin. Cell Dev. Biol.* 20:931-941.

Wong, W., and J.D. Scott. 2004. AKAP signalling complexes: focal points in space and time. *Nature reviews. Molecular cell biology*. 5:959-970.

Xiong, J.P., T. Stehle, R. Zhang, A. Joachimiak, M. Frech, S.L. Goodman, and M.A. Arnaout. 2002. Crystal structure of the extracellular segment of integrin alpha Vbeta3 in complex with an Arg-Gly-Asp ligand. *Science*. 296:151-155.

Yednock, T.A., C. Cannon, L.C. Fritz, F. Sanchez-Madrid, L. Steinman, and N. Karin. 1992. Prevention of experimental autoimmune encephalomyelitis by antibodies against alpha 4 beta 1 integrin. *Nature*. 356:63-66.

Yoshida, K., and T. Soldati. 2006. Dissection of amoeboid movement into two mechanically distinct modes. *J. Cell Sci.* 119:3833-3844.

Zimmerman, N.P., S.N. Kumar, J.R. Turner, and M.B. Dwinell. 2012. Cyclic AMP dysregulates intestinal epithelial cell restitution through PKA and RhoA. *Inflammatory bowel diseases*. 18:1081-1091.

Wei-Chien Hung

39 w Lexington st #407, Baltimore, MD 21201
C: 443-931-2849
wayne8000@gmail.com

EDUCATION and TRAINING

PhD candidate, Chemical and Biomolecular Engineering ***09/2009 ~ 03/2014***

- *Johns Hopkins University, Baltimore, Maryland*
- Cumulative GPA: 3.9
- Advisor: Dr. Konstantinos Konstantopoulos

Master of Science, Chemical Engineering ***08/2007 ~ 08/2009***

- *Johns Hopkins University Bloomberg School of Public Health, Baltimore, Maryland*
- MHS in Bioinformatics
- Advisor: Dr. Fernando Pineda

Bachelor of Science, Chemical Engineering ***09/2002 ~ 06/2007***

- Missouri University-Columbia
- B.S. in Biochemistry, Minor in Mathematics
- Cumulative GPA: 3.81

TECHNICAL PROFICIENCIES

Biology-related

Fluorescent Microscopy, Confocal Microscopy, Cell culture, Virus transfection/transduction, High throughput and high content assays, Western Blot, Microfluidic devices, Flow cytometry (FACS)

Analytical chemistry-related

Scanning Electron Microscope (SEM), Tunneling Electron Microscope (TEM), Energy Dispersive X-ray Spectroscopy (XRD), Optical Spectroscopy, Raman Spectroscopy, Thermogravimetric Analysis (TGA), Fourier Transform Infrared Spectroscopy (FTIR), Photolithography, Atomic Force Microscopy

PROFESSIONAL EXPERIENCE

Predoctoral research fellow

10/2009 ~ Present

Physical Science - Oncology Center, Johns Hopkins University

- **Topic: Distinct signaling mechanisms regulate migration in unconfined versus confined spaces:** Used novel microchannel assay to probe the alpha4 integrin mediated signaling and the crosstalk between Rac1 and Myosin II pathway.
- **Topic: Fluid Shear Promotes Chondrosarcoma Cell Invasion by Activating Matrix Metalloproteinase-12 via IGF-2- and VEGF-Signaling Pathways:** Develop unique micro-channel based invasion and migration assay to simulate in vivo cancer metastasis regulated by MMP-12 pathway.
- **Topic: Cell migration adapts physical environments via modulating protein kinase A activity:** Applied FRET (fluorescence resonance energy transfer) based PKA biosensor to probe global/local PKA cellular activity in response to different degrees of physical confinement.

- **General:** Provide advise and mentor 6 undergraduate, master and graduate students on their research; Collaborate with several postdocs, pathologists, oncologists, and cell biologist from Johns Hopkins medical school and continue developing new projects; Maintain safe laboratory environment as lab safety officer.

Department of Biostatistics
9/2007 ~ 9/2009
Johns Hopkins University Bloomberg School of Public Health

- **Topic:** developed a mosquito-human interacting model to predict the incidence of malaria.

PUBLICATIONS (6 publications; 100 citations, until September 2014)

- **Hung WC**, Chen SH, Paul CD, Stroka KM, Lo YC, Yang JT, Konstantopoulos K. (2013) "Distinct signaling mechanisms regulate migration in unconfined versus confined spaces" J Cell Biol. 202(5):807-24 **(highlighted by J Cell Biol; selected by F1000Prime)**
- Wang P*, Chen SH*, **Hung WC*** (***equally contributed**), Paul CD, Zhu F, Guan P, Huso DL, Kontrogianni- Konstantopoulos A, Konstantopoulos K "Fluid Shear Promotes Chondrosarcoma Cell Invasion by Activating Matrix Metalloproteinase-12 via IGF-2- and VEGF-Signaling Pathways" Oncogene, in press.
- **Hung WC***, Jessica Yang* (***equally contributed**), Gu ZZ, Yankaskas C, Chaing J, Zhang J, Yang JT, Konstantopoulos K."Cell migration adapts physical environments via modulating protein kinase A activity", in preparation.
- Chen SH, **Hung WC**, Wang P, Paul CD, Konstantopoulos K. (2013)"Mesothelin binding to CA125/MUC16 promotes pancreatic cancer cell motility and invasion via MMP-7 activation" Sci Rep. 3:1870
- Norris LC, Fornadel CM, **Hung WC**, Pineda FJ, Norris DE (2010) "Frequency of multiple blood meals taken in a single gonotrophic cycle by Anopheles arabiensis mosquitoes in Macha, Zambia." Am J Trop Med Hyg. 83(1):33-7
- Tong Z, Balzer EM, Dallas MR, **Hung WC**, Stebe KJ, Konstantopoulos K (2012) "Chemotaxis of cell populations through confined spaces at single-cell resolution" PLoS One. 7(1):e29211
- Balzer EM, Tong Z, Paul CD, **Hung WC**, Stroka KM, Boggs AE, Martin SS, Konstantopoulos K (2012) "Physical confinement alters tumor cell adhesion and migration phenotypes" FASEB J. 26(10):4045-56

HONORS AND ACTIVITY

- Dean list from Missouri University-Columbia (2002-2007)
- Golden Key honor society
- Phi Beta Kappa honor society
- Article selected by F1000Prime "**Distinct signaling mechanisms regulate migration in unconfined versus confined spaces**"

TEACHING EXPERIENCE

Teaching Assistant ***01/2012 – 05/2012***
Department of Chemical and Biomoleuclar Engineering, *Johns Hopkins University, Baltimore, MD*
Course: Transport Phenomena – Fluid Dynamics, Heat, and Mass Transfer

- Hold review sections and homework recitations for eighty undergraduate students every two weeks

Teaching Assistant ***01/2008 – 05/2008***

Department of Biostatistics, *Johns Hopkins University, Baltimore, MD*

Course: General Biostatistics

- Supervised twenty graduate students from different departments to develop general biostatistics skill

Affiliations and Activities

- Chemical and Biomolecular Engineering department (Johns Hopkins University), GSLC committee (2010)
- Taiwanese Students Association Chair assistant (2010)
- INBT (institute of Nano-biotechnology) mini-symposium convener (2012)